Wilson, P.A., Lyle, M., and Firth, J.V. (Eds.)
Proceedings of the Ocean Drilling Program, Scientific Results Volume 199

2. Integrated Stratigraphic Correlation and Improved Composite Depth Scales for ODP Sites 1218 and 1219[1]

Heiko Pälike,[2] Ted Moore,[3] Jan Backman,[4] Isabella Raffi,[5] Luca Lanci,[6, 7] Josep M. Parés,[3] and Thomas Janecek[8]

[1]Pälike, H., Moore, T., Backman, J., Raffi, I., Lanci, L., Parés, J.M., and Janecek, T., 2005. Integrated stratigraphic correlation and improved composite depth scales for ODP Sites 1218 and 1219. *In* Wilson, P.A., Lyle, M., and Firth, J.V. (Eds.), *Proc. ODP, Sci. Results,* 199, 1–41 [Online]. Available from World Wide Web: <http://www-odp.tamu.edu/publications/199_SR/VOLUME/CHAPTERS/213.PDF>. [Cited YYYY-MM-DD]
[2]Southampton Oceanography Centre, School of Ocean and Earth Science, European Way, Southampton SO14 3ZH, UK. **h.palike@soton.ac.uk**
[3]Geological Sciences, University of Michigan, 2534 C.C. Little Building, 425 East University Avenue, Ann Arbor MI, 48109-1063, USA.
[4]Department of Geology and Geochemistry, Stockholm University, 10691 Stockholm, Sweden.
[5]Dipartimento di Scienze della Terra, Universitario "G. D'Annunzio," Campus Universitario, Via dei Vestini 31, 66013 Chieti Scalo, Italy.
[6]Istituto di Dinamica Ambientale, Universita' di Urbino Localita Crocicchia, 61029 Urbino, Italy.
[7]Department of Geological Sciences, Rutgers University, Piscataway NJ 08854, USA.
[8]IODP Management International, Inc., 1899 L Street, Northwest, Suite 200, Washington DC 20036, USA.

Initial receipt: 19 April 2004
Acceptance: 16 November 2004
Web publication: 2 June 2005
Ms 199SR-213

ABSTRACT

During Ocean Drilling Program Leg 199 a high-resolution (~1–2 cm/k.y.) biogenic sediment record from the late Paleocene to the early Miocene was recovered, containing an uninterrupted set of geomagnetic chrons as well as a detailed record of calcareous and siliceous biostratigraphic datum events. Shipboard lithologic proxy measurements and shore-based determinations of $CaCO_3$ revealed regular cycles that can be attributed to climatic forcing. Discovering drill sites with well defined magneto- and biostratigraphic records that also show clear lithologic cycles is rare and valuable and creates the opportunity to develop a detailed stratigraphic intersite correlation, providing the basis to study paleoceanographic processes and mass accumulation rates at high resolution.

Here we present extensive postcruise work that extends the shipboard composite depth stratigraphy by providing a high-resolution revised meters composite depth (rmcd) scale to compensate for depth distortion within individual cores. The depth-aligned data were then used to generate stacked records of lithologic proxy measurements. Making use of the increased signal-to-noise ratio in the stacked records, we then proceeded to generate a detailed site-to-site correlation between Sites 1218 and 1219 in order to decrease the depth uncertainty for magneto- and biostratigraphic datums. Stacked lithologic proxy records in combination with discrete measurements of $CaCO_3$ were then exploited to

calculate high-resolution carbonate concentration curves by regression of the multisensor track data with discrete measurements. By matching correlative features between the cores and wireline logging data, we also rescaled our core rmcd back to in situ depths. Our study identifies lithology-dependent core expansion due to unloading as the mechanism of varying stratigraphic thicknesses between cores.

INTRODUCTION

During Ocean Drilling Program (ODP) Leg 199 (Fig. F1), a series of eight sites was drilled in the central to eastern equatorial Pacific. The cruise was designed as a latitudinal transect, targeting sediments on Anomaly 25, just prior to the Paleocene/Eocene boundary. One of the primary objectives of ODP Leg 199 was the recovery of continuous, undisturbed, and high-resolution sediment records from the Paleogene. Throughout the entire Oligocene and parts of the Eocene and Miocene, high-resolution lithologic data from Site 1218 (8°53.378′N, 135°22.00′W; 4828 m present-day water depth) and Site 1219 (7°48.019′N, 142°00.940′W; 5063 m present-day water depth) show a very high correlation, at centimeter to decimeter length scales, even though the two sites are separated laterally by >740 km. For this contribution, we developed detailed and improved hole-to-hole, new site-to-site, and core-to-log correlations for Sites 1218 and 1219, thus providing stratigraphic information that forms the basis for additional studies.

For paleoceanographic interpretations and analysis of depth and time series, it is crucial that one is able to demonstrate the continuity of a given record. Thus, one has to be able to recognize the presence of hiatuses in the sedimentary record, and it is necessary to compensate for the limitations that result from the technology used to recover deep-marine sediment cores. ODP sediment cores are typically recovered in ~9.5-m-long sections. Depending on the consistency and hardness of the sediment encountered during drilling, different recovery methods are used (e.g., advanced piston coring [APC], extended core barrel [XCB] coring, or rotary core barrel coring [not used during ODP Leg 199]). Even with a nominal 100% recovery, recovery gaps are present between successive cores. These are at least on the order of tens of centimeters, typically 1–2 m, and rarely are the same strata recovered multiple times. Depending on the recovery method used, cores can also be affected by core fragmentation, slumping, core expansion due to unloading, core stretching and squeezing, and other core deformations, some of them related to the motion of the drill ship during coring (heaves, tides, etc.).

In order to obtain a complete geological record, multiple adjacent holes are cored at each site. By applying a depth offset of typically 2–5 m between cores from different holes during coring, one can then ensure that those intervals missing within a single hole can be recovered from an adjacent hole, which allows an evaluation of the length of core gaps, as well as the construction of a "spliced" representative record. Initially, each ~9.5-m-long core is assigned a depth according to the drill string length. This depth is denoted as meters below seafloor (mbsf). Subsequently, an attempt is made to correlate cores from different holes by using common features and diagnostic excursions in measurements of physical properties (bulk density, magnetic susceptibility, color reflectance, etc.) or magneto- and biostratigraphic records and events. Routinely, the depths of cores from different holes are adjusted

F1. Leg 199 drilling sites, p. 12.

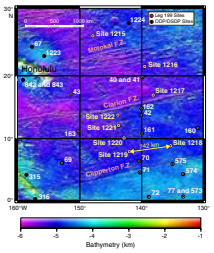

to a common depth scale by adding a constant offset over the length of each core. This new depth scale is denoted as meters composite depth (mcd) and is generated shipboard during the cruise. The methodology for this shipboard stratigraphic correlation was pioneered during Legs 94 (Ruddiman et al., 1987) and 138 (Hagelberg et al., 1992). Similar methods were employed and developed further during Legs 154 (Curry, Shackleton, Richter, et al., 1995), 162 (Jansen, Raymo, Blum, et al., 1996), 167 (Lyle, Koizumi, Richter, et al., 1997), 171B (Norris, Kroon, Klaus, et al., 1998), 189 (Exon, Kennett, Malone, et al., 2001), and 198 (Shipboard Scientific Party, 2002a). A new innovation of relating depth offsets between separate holes to precalculated tidal movements was introduced during Leg 202 (Shipboard Scientific Party, 2003).

Unfortunately, it has been frequently observed that cores are distorted in length within each ~9.5-m segment. This distortion is due to the coring methods used or to variations in accumulation rates between holes. This problem was discussed in detail by Hagelberg et al. (1995). For example, sediment inside the core can expand as a result of reduced environmental pressure following core recovery, leading to an expanded sedimentary sequence relative to its original length (Moran, 1997). The coring technology can also lead to sediment distortion (Skinner and McCave, 2003). The distortion in depth implies that geological events that are obviously synchronous in time, such as volcanic ash layers, are potentially not correctly aligned on the mcd scale.

This situation is not satisfactory, as far as a detailed stratigraphic correlation is concerned. Two strategies can be used to alleviate this problem. The one that is used shipboard is to construct a "spliced" record from available data by using the mcd scale and by switching the sampling between records from different holes. The splicing procedure requires a decision to be made with respect to what constitutes the "best" (or most representative) track and will depend on the purpose of the particular investigation. For example, one might want to choose, where available, the longest possible track down the core sequence, assuming that this record results in the highest possible resolution in time. Alternatively, one might want to select a "splice" that corresponds to the average increase in depth if, for example, the aim is the reconstruction of sediment flux variations. These arguments were put forward previously during Leg 171B (Shipboard Scientific Party, 1998).

An alternative to the construction of a "spliced" record is the calculation of a stacked record, treating data from different holes as the realization of the same geological section. The procedure for the generation of a common depth scale that allows stretching and squeezing on a centimeter scale was pioneered by Hagelberg et al. (1995) and results in a "revised meters composite depth" (rmcd) scale. In this case, it is necessary to align individual features between different holes at high resolution, allowing differential stretching and squeezing of depths within individual holes. This strategy was also employed by Pälike et al. (2001). As the rmcd scale implies that cores from individual holes are aligned not only at specific depths but ideally along the entire record, it is possible to "stack" (average) data from different cores covering the same stratigraphic interval. This method can facilitate the generation of an enhanced "signal-to-noise" ratio (i.e., "noise" in the data that is independent of the location of the holes can be reduced by averaging several measurements from the same stratigraphic level). New, improved sampling splices can be generated according to the rmcd scale, minimizing sampling waste and analytical time.

Figure F2 illustrates the relationship between the mbsf, mcd, and rmcd scales. In the left panel, gamma ray attenuation (GRA) bulk density data from three holes are shown on the shipboard mbsf depth scale, as determined by the length of the drill string. Note that features that clearly represent identical stratigraphic horizons are slightly offset from each other. The middle panel shows data on a common (mcd) scale as determined shipboard. This common depth scale is generated by matching one single point in depth between individual cores, not allowing any stretching and/or squeezing of depths within a single core. The shipboard mcd scale is used to create a single representative sample track, switching between holes ("splice"). The right panel shows an example of the revised composite depth scale developed here. Note that data are aligned on shorter-length scales compared to the shipboard mcd scale. The aligned data can then be used to generate a stacked record, reducing the noise component in the data (right panel). If the available data only allow an ambiguous or imprecise correlation, or if multiple hole data were unavailable, no additional depth adjustments were made. In this case, the cumulative offset remains constant for all subsequent cores.

F2. Illustration of depth scale concept, p. 13.

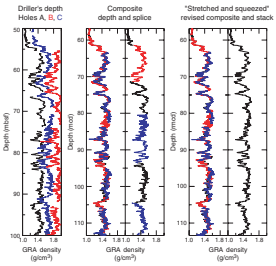

MATERIALS

The data used for generating our new revised meters composite depth scale were multisensor track (MST) data (magnetic susceptibility, GRA bulk density, and color reflectance parameters [L*, a*, and b* color space]), paleomagnetic properties measured shipboard, and additional postcruise discrete measurements of $CaCO_3$ content from Sites 1218 and 1219. Three holes were drilled at Site 1218 and two were drilled at Site 1219. Hole 1219B was abandoned prematurely, due to a stuck core barrel. The MST data were lightly pruned to remove incorrect values, which were found to occur mostly at the ends of cores, as well as in disturbed intervals determined shipboard by visual inspection of the split cores (Shipboard Scientific Party, 2002b, 2002c). Where multiple copies of the same stratigraphic interval were available, comparisons between data from different holes allowed the identification of additional outliers.

RESULTS

Hole-to-Hole Correlation for Sites 1218 and 1219

Our strategy for developing rmcd hole-to-hole correlations for Sites 1218 and 1219 was to keep the rmcd scale similar to the original shipboard splice mcd scale, where possible, in order to facilitate comparison with shipboard results and to ease the creation of alternative sediment sampling plans. Thus, where multiple copies of the same stratigraphic interval were recovered, our revised composite depths (rmcd) are identical with the shipboard composite depths of the core that is part of the original shipboard splice, whereas the other cores were finely adjusted to give the best match for all the holes on a centimeter to decimeter scale. We achieved this aim for Site 1218. For Site 1219, we had to correct some shipboard composite depth scale mismatches but kept most of the shipboard correlations intact. Following shipboard practice for intervals recovered in only one hole, we offset mcd and rmcd depths by

a nominal ~1.1 m, according to the average observed length increase of the mcd/rmcd depth scale. The complete data sets, plotted on the new rmcd scale, are shown in Figures F3 and F4. In addition to the MST data, aligned on the rmcd scale, we also show the stacked records as superimposed dashed lines; the generation of these is discussed in a separate section. We also show the points where the original splice track switches between different holes. For Site 1218, all but one original splice point (toward the very bottom) were kept. The depth adjustments within each core were made by considering all data sets. However, depending on the lithology, different types of data were more useful for this purpose: the carbonate-poorer lithologic Units I, III, and IV (Shipboard Scientific Party, 2002a) were more easily matched using the magnetic susceptibility data, whereas for the carbonate-rich Unit II, all data proved equally useful. The depth tables that relate mbsf, mcd, and our new rmcd scales are given as Table T1 for Site 1218 and Table T2 for Site 1219. Depths were linearly interpolated between individual tie points. We note that the improved stratigraphic hole-to-hole correlation was relatively straightforward for intervals of intermediate carbonate content. For carbonate-poor intervals, characterized by low lightness and bulk density values and high magnetic susceptibility values, matches were based mostly on the magnetic susceptibility measurements.

Stacked MST Data Sets for Sites 1218 and 1219

One of the main reasons for generating a detailed new rmcd depth scale is that after alignment to this scale it is possible to stack data from different holes, thus increasing the signal-to-noise ratio. For example, color reflectance data are acquired by spot measurements with a footprint of ~4 mm². Thus, processes such as bioturbation or uneven surfaces of split cores will produce noise in the data. The stacking process allows us to reduce this noise for all data sets and provides a more representative record. We generated stacked data sets for magnetic susceptibility, color reflectance (L*, a*, and b* color space), and GRA bulk density as follows. The pruned data, aligned on the rmcd scale, were first visually inspected for occurrences where data from one hole were significantly different from the other holes. If those data points were clearly outliers, they were removed. We then resampled data from all holes with a common 2-cm sampling step where available, using a Gaussian smoothing window with a half-width of 5 cm. The resampling is necessary, as the process of "stretching and squeezing" within cores implies that data measurements are no longer spaced equally in depth, and data from different holes are also not sampled at identical depths. The width of the smoothing window was chosen so as to preserve variations of the lithologic measurements that were common between data from separate holes. As the average sedimentation rates were between ~0.5 and 2 cm/k.y. throughout the Site 1218 and 1219 records, this smoothing process preserves any information with timescales longer than a few thousand years and is of the same order as that applied by the magnetic susceptibility loop during data acquisition. The smoothed data were then averaged if data were available from more than one hole or taken from a single hole. The stacked data sets are available in electronic form, as they are too large to be included as complete tables here. However, the format of the data tables is shown in Table T3 for Site 1218 and Table T4 for Site 1219.

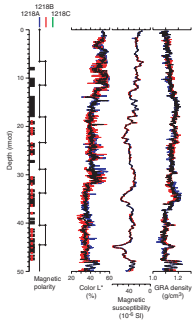

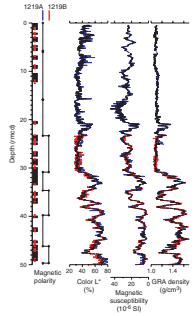

Site-to-Site Correlation

It is important to stress that data correlated from one site alone might not be sufficient to identify hiatuses in the record, as a particular stratigraphic interval might only be recovered in a single hole. One of the strengths of stratigraphic correlations that were performed with data from ODP Legs 138 and 154 (Shackleton et al., 1995; Shackleton and Crowhurst, 1997; Shackleton et al., 1999) was that these correlations were not only achieved with data from one particular location, but with data from different sites. This approach allowed the detection of several hiatuses that otherwise would have remained unnoticed. We follow this pioneering work by performing additional site-to-site correlations for ODP Sites 1218 and 1219. Figure F5 illustrates how well the data between Sites 1218 and 1219 can be matched for an interval in the upper Oligocene/lower Miocene. Table T5 provides the tie points that match Site 1219 depths (in rmcd) to those of Site 1218. We applied a linear interpolation of depths between these tie points. The matching of data from 1219 to 1218 shows that individual features of the MST data can be matched on a centimeter to decimeter scale, an observation that is truly astonishing, given the large distance (~740 km) between Sites 1218 and 1219. We note that the comparison of data from Sites 1218 and 1219 suggests that both sedimentary sequences are complete and not interrupted by any hiatuses, at least on the scale of the lateral separation of the two sites.

F5. Site-to-site correlation of MST data, p. 26.

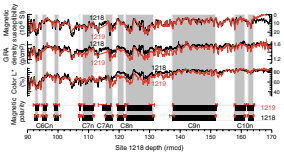

T5. Mapping tie points from Site 1219 to Site 1218 rmcd, p. 35.

Magneto- and Biostratigraphic Integration

Because data from the two sites match so well, we can now proceed to use this match to extrapolate magneto- and biostratigraphic datum events between sites. This approach yields two important benefits. First, we can evaluate, and reduce, the uncertainty in depth for datum events that cooccur at both sites. We can also evaluate small potential latitudinal differences for biostratigraphic events, as Sites 1218 and 1219 were at slightly different paleolatitudes at any given time (Lyle, Wilson, Janecek, et al., 2002). Second, for datum events that were only determined for one of the two sites, we can use the newly developed match of rmcd depth scales from Sites 1218 and 1219 to predict the position of these datum events for the site where it was not determined, thus improving the database available for generating detailed age models.

The depth determinations for magnetostratigraphic events presented here are based on shipboard magnetic data that were available at the time. We note that additional postcruise work has been carried out for some intervals of Sites 1218 and 1219 (Lanci et al., 2004), which will further reduce the depth uncertainty for these events. Table T6 lists magnetostratigraphic events interpreted for Sites 1218 and 1219 on our new rmcd scale, together with depth uncertainty estimates. We note that the correlation between Sites 1218 and 1219 is very good for the cabonate-rich interval (~55–240 rmcd for Site 1218). Above 55 rmcd, the identification and correlation of magnetic reversals is less certain. Table T6 also gives depths for Site 1219 as Site 1218 equivalents, using our site-to-site correlation. There are two examples where our site-to-site correlation gives information that data from the two sites on their own were unable to provide. Polarity Chron C11n, for example, was not identified with confidence in the shipboard magnetostratigraphic data for Site 1219; our match allows the determination of the equivalent stratigraphic interval for Site 1219 from data from Site 1218. Sec-

T6. Integrated magnetostratigraphy from Sites 1218 and 1219, p. 36.

ond, no magnetostratigraphic data are available from Site 1218 below Chron C12n, as the lithologic nature of sediments required a switch from the APC coring system to XCB. However, our site-to-site correlation results in depth estimates for Chrons C13n through C20n for Site 1218 by extrapolation from Site 1219, thus improving our ability to constrain age models. There are several additional examples where core breaks or core disturbance increased the depth uncertainty of magnetic reversals at one site that can now be further reduced by using our newly developed site-to-site correlation.

As was the case for the magnetostratigraphic data, we can also improve our available database of biostratigraphic datums by hole-to-hole and site-to-site correlation. The detailed determination of radiolarian datum events is given elsewhere (**Nigrini et al.,** this volume). Calcareous nannofossil datum events, some of them improved from the original shipboard information, are listed in Table **T7** for Site 1218 and Table **T8** for Site 1219. For Site 1219, we also give equivalent depths for Site 1218, as determined by the tie points listed in Table **T5.** The integrated correlation of magneto- and biostratigraphic datum events to lithologic cycles from Sites 1218 and 1219 forms the basis for the development of an improved age model for the two sites.

T7. Site 1218 calcareous nannofossils on rmcd scale, p. 39.

T8. Site 1219 calcareous nannofossils on rmcd scale, p. 40.

Estimates of $CaCO_3$ Contents from Multisensor Track Data

The development of stacked MST data sets for Sites 1218 and 1219, together with shipboard and additional determinations of $CaCO_3$ content for the two sites, allowed us to generate new high-resolution "estimated" carbonate content, based on a regression between lower-resolution direct measurements of $CaCO_3$ and the stacked MST data. A high-resolution $CaCO_3$ record is valuable, as it allows the investigation of depth- and latitude-dependent dissolution and productivity patterns as a function of the carbonate compensation depth (CCD). Using the stacked data sets of magnetic susceptibility, GRA bulk density, and the three color reflectance parameters L*, a*, and b*, we first extracted the dominant variation of these five parameters by principal component analysis. We then used a polynomial regression between the three leading principal components and measured $CaCO_3$ values (e.g., Coxall et al., 2005), to develop high-resolution estimates of carbonate content from ~60 to 241 m depth on the Site 1218 rmcd scale, covering the earliest Oligocene to early/middle Miocene. Our results for Sites 1218 and 1219 are illustrated in Figure **F6.** Based on a comparison between the measured and estimated values, we determined the uncertainty of our estimated $CaCO_3$ values to be on the order of 10%–15%. This uncertainty is lower for the interval from ~110 to 240 rmcd, but we note that the estimated values for Site 1218 are slightly (~10%) too low for the interval between 60 and 100 rmcd. Although it is possible to improve the match of measured and estimated $CaCO_3$ values by calculating regressions over shorter subintervals, this also results in undesirable jumps in the estimated curves. A separate study (**Vanden Berg and Jarrard,** this volume) derived estimated calcite, opal, and terrigenous components by regression with light absorption spectroscopy data. We note that these two methods yielded similar results.

F6. Estimated $CaCO_3$ content regressions, p. 27.

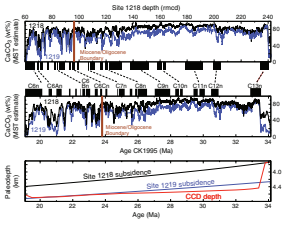

In combination with an astronomical age calibration of data from Sites 1218 and 1219 (Wade and Pälike, 2004; H.K. Coxall et al., 2005, unpubl. data), our estimated $CaCO_3$ values combined with the stacked

GRA bulk density estimates allow us to calculate more detailed mass accumulation rates of calcium carbonate for Sites 1218 and 1219. One interesting aspect of carbonate accumulation for the two sites arises by comparison with the tectonic subsidence histories of the two sites. Figure F6 illustrates that although $CaCO_3$ is quite similar between Sites 1218 and 1219 throughout most of the Oligocene, Site 1219 shows a stronger decrease in $CaCO_3$ values as this site approaches the depth of the CCD (also see Rea and Lyle, 2005, and Coxall et al., 2005, for more detailed discussion of the CCD development).

Matching Stacked Core Data to Wireline Logging Data

One final aspect of our integrated correlation effort is the calibration of our new rmcd scale to logging data. Similar procedures have been employed during previous ODP legs (Harris et al., 1995). The observation that mcd and rmcd scales are expanded compared to the mbsf scale arising from the length of the drill string has important consequences on properties that rely on absolute sediment thicknesses, such as sedimentation and mass accumulation rate estimates and synthetic seismogram studies. The hole-to-hole and site-to-site correlations have already demonstrated that the expansion in length of the rmcd scale compared to the mbsf scale is largely due to lithology-dependent core expansion caused by unloading. This view is confirmed by **Rea and Gaillot** (this volume), who computed core rebound coefficients by comparison of wireline in situ depths with core depths. Figure F7 illlustrates how stacked core data can be matched well to downhole logging data. The comparison of logging data with core data rests largely on measurements that represent the sediment porosity and/or density. Table T9 provides the tie points that match Site 1218 depths (in rmcd) to in situ logging depths (lmbsf). We observe that, on average, the in situ logging depth is ~89% of the rmcd scale, indicating that core expansion is on the order of 11%. One important result of our core-logging data comparison is the observation that both Formation MicroScanner and lithodensity logging data show an intermediate step in the transition visible at ~213 lmbsf, at the base of Chron C13n. Sediment data also show this two-step transition but were only recovered in a core from a single hole (1218C). Thus, our match of logging data and core data can confirm that this step is an in situ feature at Site 1218 and not a coring artifact. We note that no correlation of logging data to core data was possible above ~70 mbsf, as the drill string was not removed completely during logging. We also observe that the logging data from Site 1218 are less noisy than those from Site 1219, and a match of Site 1219 to true depth is more easily accomplished by employing our site-to-site correlation in combination with the Site 1218 logging data than by using the Site 1219 logging data.

F7. Stacked gamma ray attenuation bulk density data, p. 28.

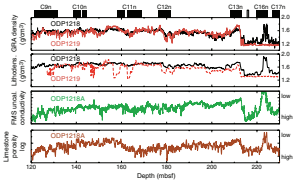

T9. Mapping tie points from Site 1218 rmcd to wireline log mbsf, p. 41.

SUMMARY

We performed a comprehensive hole-to-hole and site-to-site correlation for Sites 1218 and 1219, using physical property measurements. We compensated for depth distortions within cores by developing detailed "stretched and squeezed" revised composite depth scales for ODP Sites 1218 and 1219, two sites that are separated laterally by more than ~740 km. Our new, improved rmcd scale allowed the generation of

stacked lithologic parameter records, with a reduced noise component. A detailed site-to-site correlation of Sites 1218 and 1219 is possible down to the decimeter scale (across ~740 km), allowing improvement and verification of biostratigraphic and paleomagnetic events. These integrated stratigraphic datum events form the basis for additional (astronomical) age scale developments and intercalibrations of magneto- and biostratigraphic datum points. Stacked MST data from the two sites, combined with additional chemical determinations of $CaCO_3$ content, allowed the generation of high-resolution "estimated" $CaCO_3$ curves. By matching stacks of core physical property measurements to downhole logging data, we were able to estimate in situ depths and to correct for core expansion that we find to be due to sediment unloading during coring.

ACKNOWLEDGMENTS

This research used samples and data provided by the Ocean Drilling Program (ODP). ODP is sponsored by the U.S. National Science Foundation (NSF) and participating countries under the management of Joint Oceanographic Institutions (JOI), Inc. Funding for this research was provided to H.P. by the Swedish Research Council (VR) and the UK Natural Environment Research Council (NERC).

REFERENCES

Cande, S.C., and Kent, D.V., 1995. Revised calibration of the geomagnetic polarity timescale for the Late Cretaceous and Cenozoic. *J. Geophys. Res.,* 100:10.1029/94JB03098.

Coxall, H.K., Wilson, P.A., Pälike, H., Lear, C.H., and Backman, J., 2005. Rapid stepwise onset of Antarctic glaciation and deeper calcite compensation in the Pacific Ocean. *Nature (London, U. K.),* 433:10.1038/nature03135.

Curry, W.B., Shackleton, N.J., Richter, C., et al., 1995. *Proc. ODP, Init. Repts.,* 154: College Station, TX (Ocean Drilling Program).

Exon, N.F., Kennett, J.P., Malone, M.J., et al., 2001. *Proc. ODP, Init. Repts.,* 189 [Online]. Available from World Wide Web: <http://www-odp.tamu.edu/publications/189_IR/189ir.htm>. [Cited 2004-04-10]

Hagelberg, T.K., Pisias, N.G., Shackleton, N.J., Mix, A.C., and Harris, S., 1995. Refinement of a high-resolution, continuous sedimentary section for studying equatorial Pacific Ocean paleoceanography, Leg 138. *In* Pisias, N.G., Mayer, L.A., Janecek, T.R., Palmer-Julson, A., and van Andel, T.H. (Eds.), *Proc. ODP, Sci Results,* 138: College Station, TX (Ocean Drilling Program), 31–46.

Hagelberg, T., Shackleton, N., Pisias, N., and Shipboard Scientific Party, 1992. Development of composite depth sections for Sites 844 through 854. *In* Mayer, L., Pisias, N., Janecek, T., et al., *Proc. ODP, Init. Repts.,* 138 (Pt. 1): College Station, TX (Ocean Drilling Program), 79–85.

Harris, S., Hagelberg, T., Mix, A., Pisias, N.G., and Shackleton, N.J., 1995. Sediment depths determined by comparisons of GRAPE and logging density data during Leg 138. *In* Pisias, N.G., Mayer, L.A., Janecek, T.R., Palmer-Julson, A., and van Andel, T.H. (Eds.), *Proc. ODP, Sci. Results,* 138: College Station, TX (Ocean Drilling Program), 47–57.

Jansen, E., Raymo, M.E., Blum, P., et al., 1996. *Proc. ODP, Init. Repts.,* 162: College Station, TX (Ocean Drilling Program).

Lanci, L., Parés, J.M., Channell, J.E.T., and Kent, D.V., 2004. Miocene magnetostratigraphy from equatorial Pacific sediments (ODP Site 1218, Leg 199). *Earth Planet. Sci. Lett.,* 226(1–2):207–224.

Lyle, M., Koizumi, I., Richter, C., et al., 1997. *Proc. ODP, Init. Repts.,* 167 [Online]. Available from World Wide Web: <http://www-odp.tamu.edu/publications/167_IR/167TOC.HTM>. [Cited 2004-04-10]

Lyle, M., Wilson, A., Janecek, T.R., et al., 2002. *Proc. ODP, Init. Repts.,* 199 [Online]. Available from World Wide Web: <http://www-odp.tamu.edu/publications/199_IR/199ir.htm>. [Cited 2004-04-10]

Moran, K., 1997. Elastic property corrections applied to Leg 154 sediment, Ceara Rise. *In* Shackleton, N.J., Curry, W.B., Richter, C., and Bralower, T.J. (Eds.), *Proc. ODP, Sci. Results,* 154: College Station, TX (Ocean Drilling Program), 151–155.

Norris, R.D., Kroon, D., Klaus, A., et al., 1998. *Proc. ODP, Init. Repts.,* 171B [Online]. Available from World Wide Web: <http://www-odp.tamu.edu/publications/171B_IR/171BTOC.HTM>. [Cited 2004-04-10].

Pälike, H., Shackleton, N.J., and Röhl, U., 2001. Astronomical forcing in late Eocene marine sediments. *Earth Planet. Sci. Lett.,* 193(3–4):10.1016/S0012-821X(01)00501-5.

Rea, D.K., and Lyle, M.W., 2005. Paleogene calcite compensation depth in the eastern subtropical Pacific: answers and questions. *Paleoceanography,* 20(1):10.1029/2004PA001064.

Ruddiman, W.F., Cameron, D., and Clement, B.M., 1987. Sediment disturbance and correlation of offset holes drilled with the hydraulic piston corer: Leg 94. *In* Ruddiman, W.F., Kidd, R.B., Thomas, E., et al., *Init. Repts. DSDP,* 94 (Pt. 2): Washington (U.S. Govt. Printing Office), 615–634.

Shackleton, N.J., and Crowhurst, S., 1997. Sediment fluxes based on an orbitally tuned time scale 5 Ma to 14 Ma, Site 926. *In* Shackleton, N.J., Curry, W.B., Richter, C., and Bralower, T.J. (Eds.), *Proc. ODP, Sci. Results,* 154: College Station, TX (Ocean Drilling Program), 69–82.

Shackleton, N.J., Crowhurst, S., Hagelberg, T., Pisias, N.G., and Schneider, D.A., 1995. A new late Neogene time scale: application to Leg 138 sites. *In* Pisias, N.G., Mayer, L.A., Janecek, T.R., Palmer-Julson, A., and van Andel, T.H. (Eds.), *Proc. ODP, Sci. Results,* 138: College Station, TX (Ocean Drilling Program), 73–101.

Shackleton, N.J., Crowhurst, S.J., Weedon, G.P., and Laskar, J., 1999. Astronomical calibration of Oligocene–Miocene time. *Philos. Trans. R. Soc. London, Ser. A,* 357:1907–1929.

Shipboard Scientific Party, 1998. Site 1052. *In* Norris, R.D., Kroon, D., Klaus, A., et al., *Proc. ODP, Init. Repts.,* 171B, 241–319 [Online]. Available from World Wide Web: <http://www-odp.tamu.edu/publications/171B_IR/CHAP_06.PDF>. [Cited 2004-04-10]

Shipboard Scientific Party, 2002a. Leg 198 summary. *In* Bralower, T.J., Premoli Silva, I., Malone, M.J., et al., *Proc. ODP, Init. Repts.,* 198, 1–148 [Online]. Available from World Wide Web: http://www-odp.tamu.edu/publications/198_IR/VOLUME/CHAPTERS/IR198_01.PDF. [Cited 2004-04-10]

Shipboard Scientific Party, 2002b. Site 1218. *In* Lyle, M., Wilson, P.A., Janecek, T.R., et al., *Proc. ODP, Init. Repts.,* 199, 1–126 [Online]. Available from World Wide Web: http://www-odp.tamu.edu/publications/199_IR/VOLUME/CHAPTERS/IR199_11.PDF. [Cited 2004-04-10]

Shipboard Scientific Party, 2002c. Site 1219. *In* Lyle, M., Wilson, P.A., Janecek, T.R., et al., *Proc. ODP, Init. Repts.,* 199, 1–129 [Online]. Available from World Wide Web: http://www-odp.tamu.edu/publications/199_IR/VOLUME/CHAPTERS/IR199_12.PDF. [Cited 2004-04-10]

Shipboard Scientific Party, 2003. Leg 202 summary. *In* Mix, A.C., Tiedemann, R., Blum, P., et al., *Proc. ODP, Init. Repts.,* 202, 1–145 [Online]. Available from World Wide Web: <http://www-odp.tamu.edu/publications/202_IR/VOLUME/CHAPTERS/IR202_01.PDF>. [Cited 2004-04-10]

Skinner, L.C., and McCave, I.N., 2003. Analysis and modelling of gravity and piston coring based on soil mechanics. *Mar. Geol.,* 199(1–2):181–204.

Wade, B.S., and Pälike, H., 2004. Oligocene climate dynamics. *Paleoceanography,* 19:10.1029/2004PA001042.

Figure F1. Site map of Ocean Drilling Program (ODP) Leg 199 drilling sites, on ETOPO2 bathymetry. DSDP = Deep Sea Drilling Project, F.Z. = fracture zone.

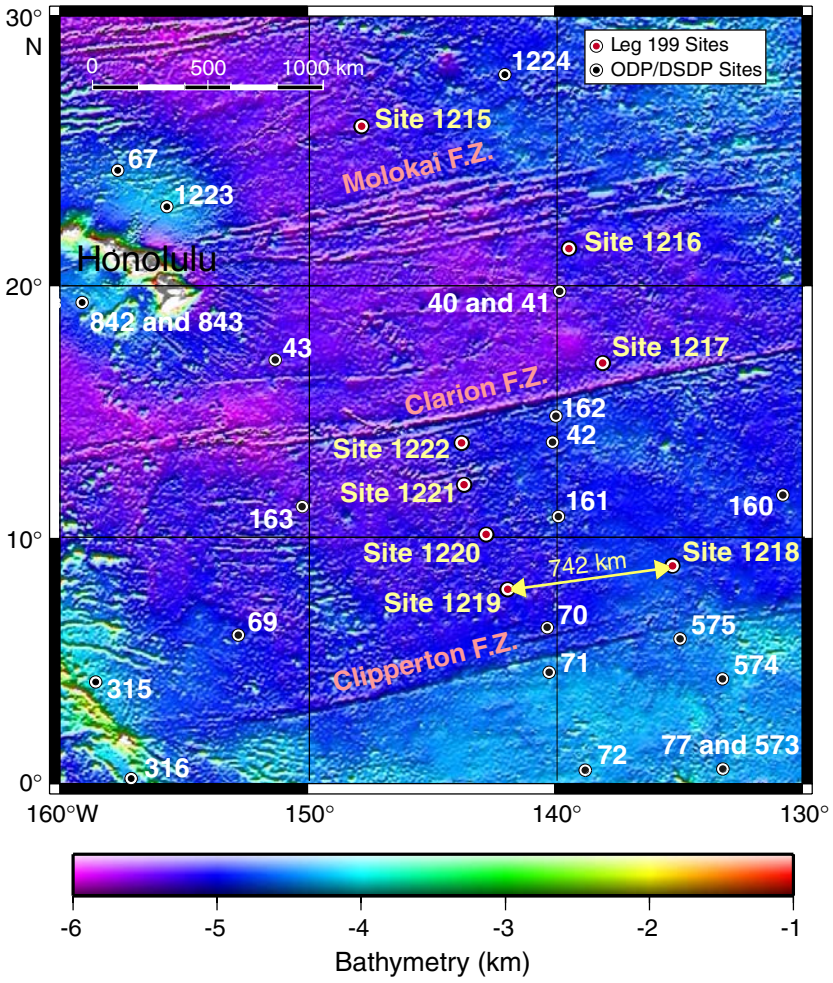

Figure F2. Illustration of mbsf, mcd, and revised mcd (rmcd) depth scale concept. GRA = gamma ray attenuation.

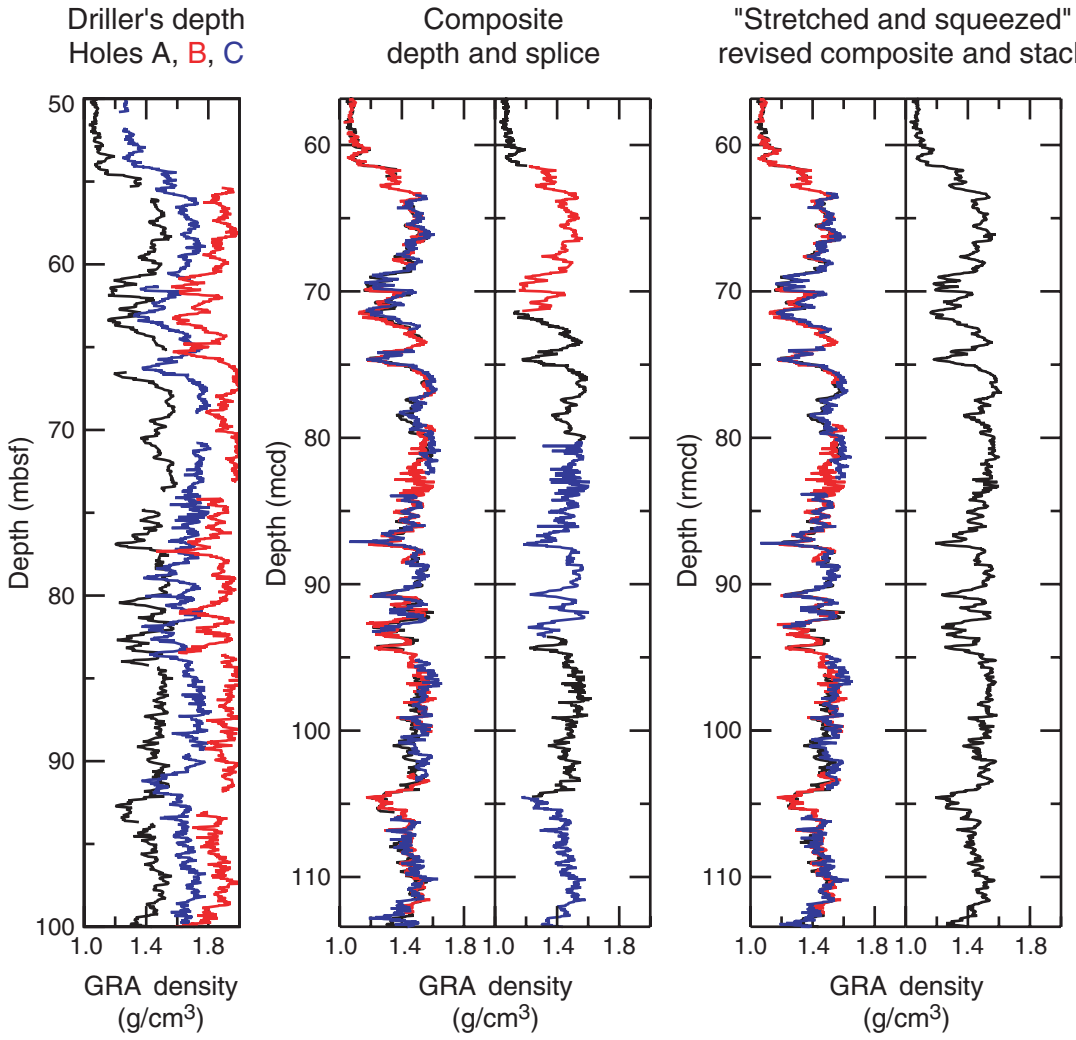

Figure F3. Site 1218 MST data on rmcd scale and stack. GRA= gamma ray attenuation. (Continued on next five pages.)

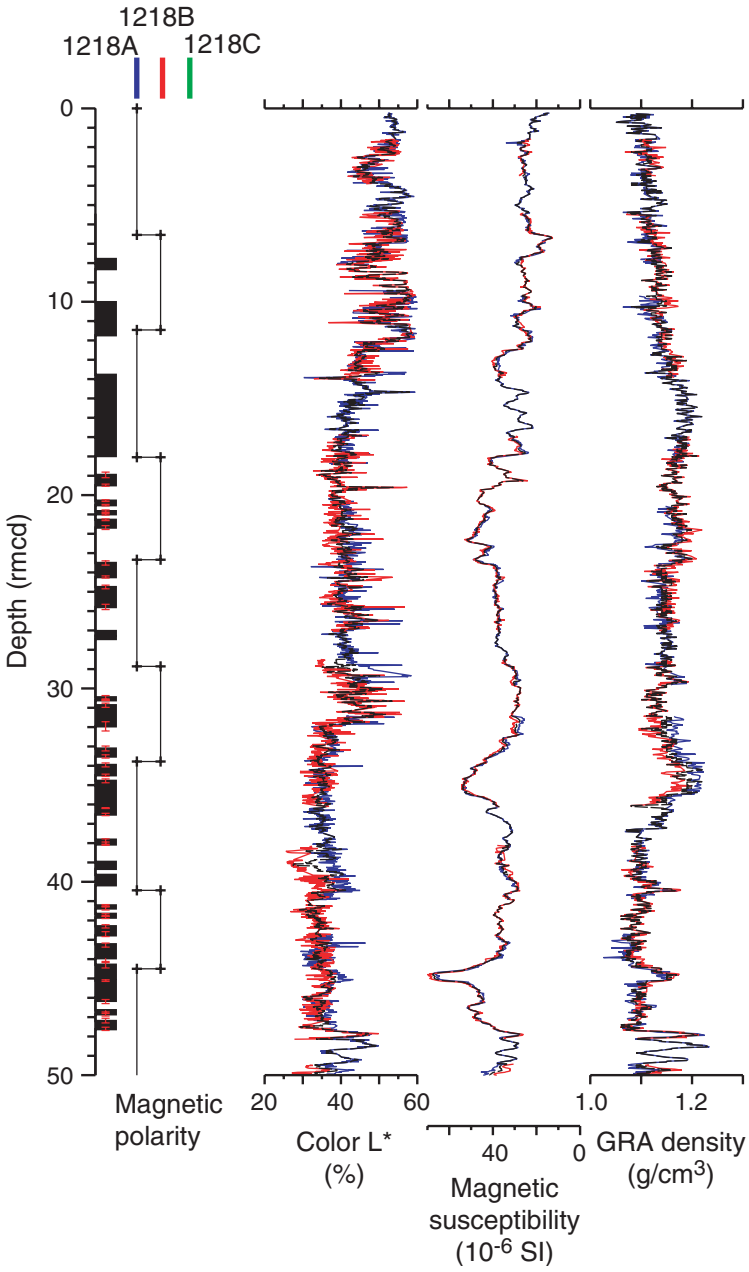

Figure F3 (continued).

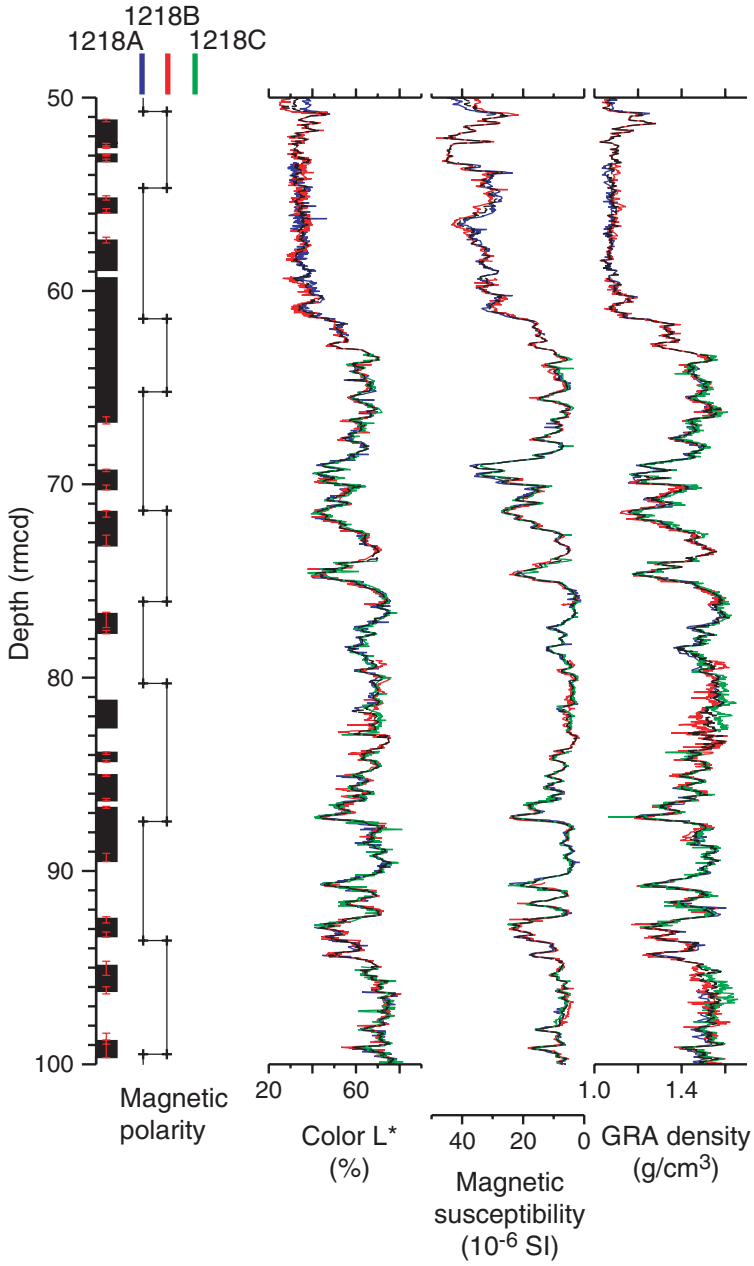

Figure F3 (continued).

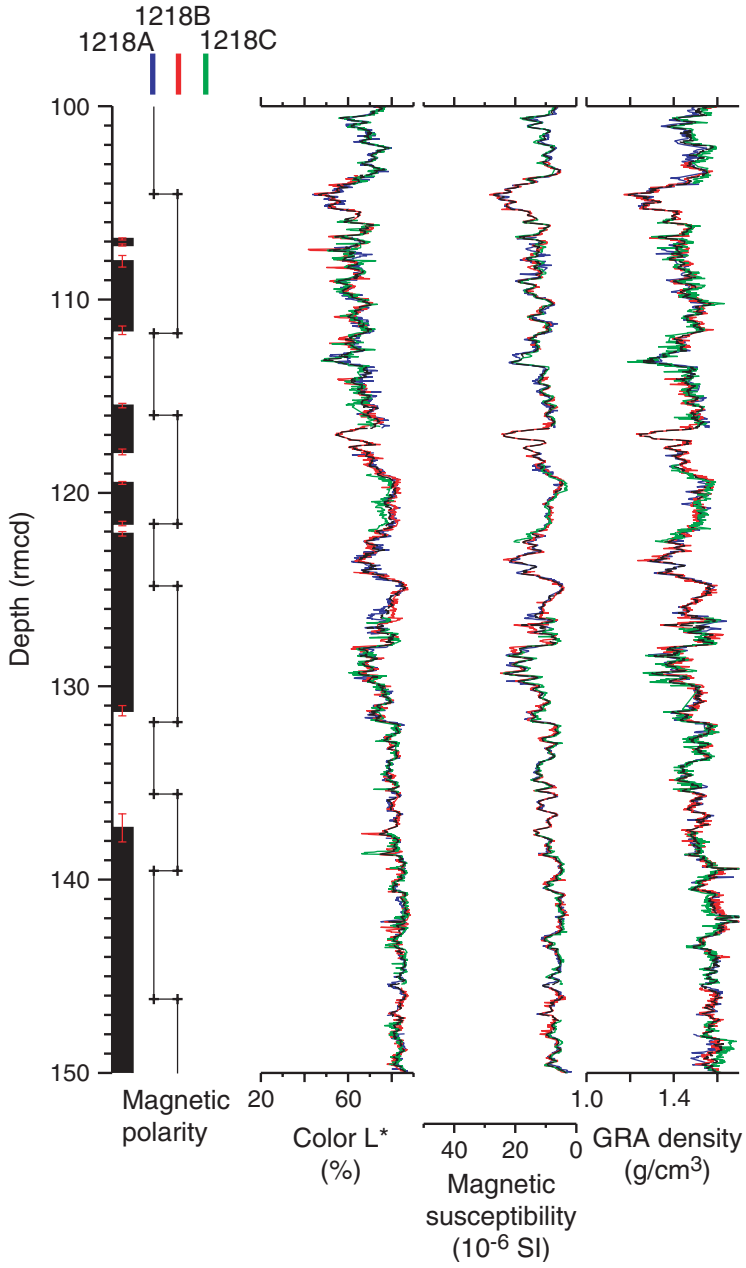

Figure F3 (continued).

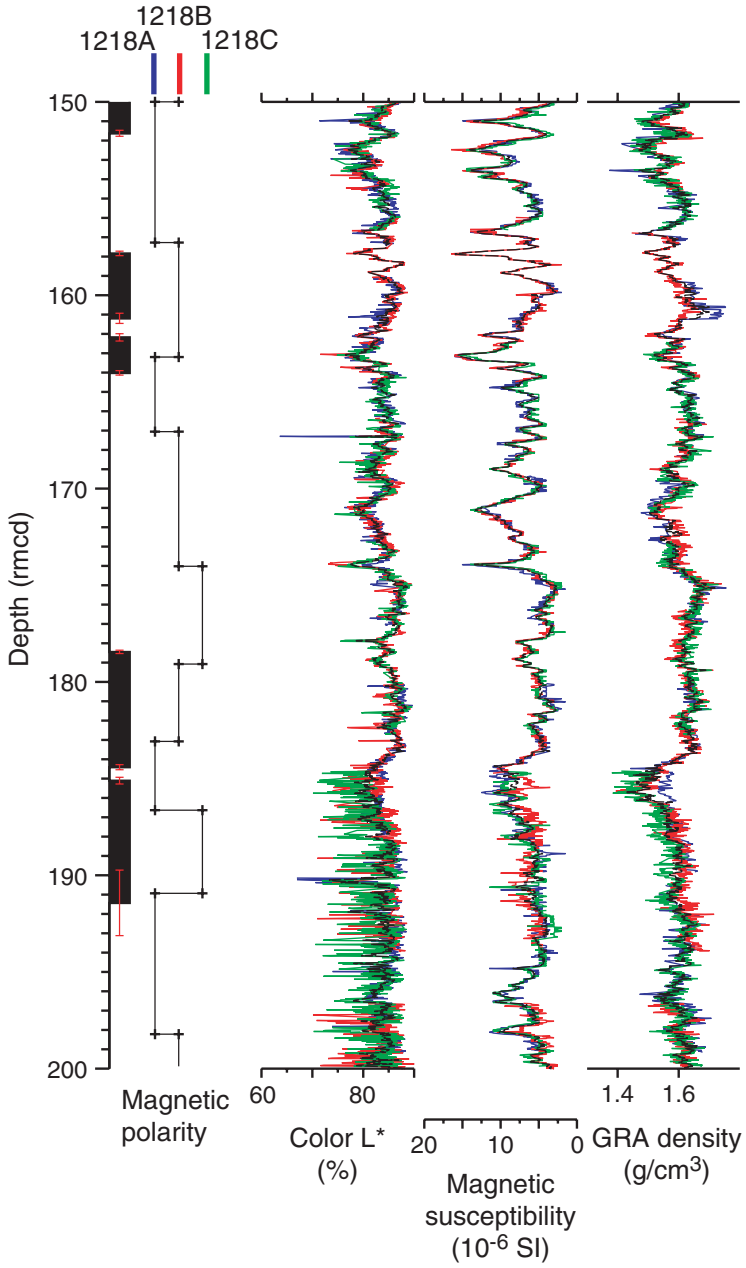

Figure F3 (continued).

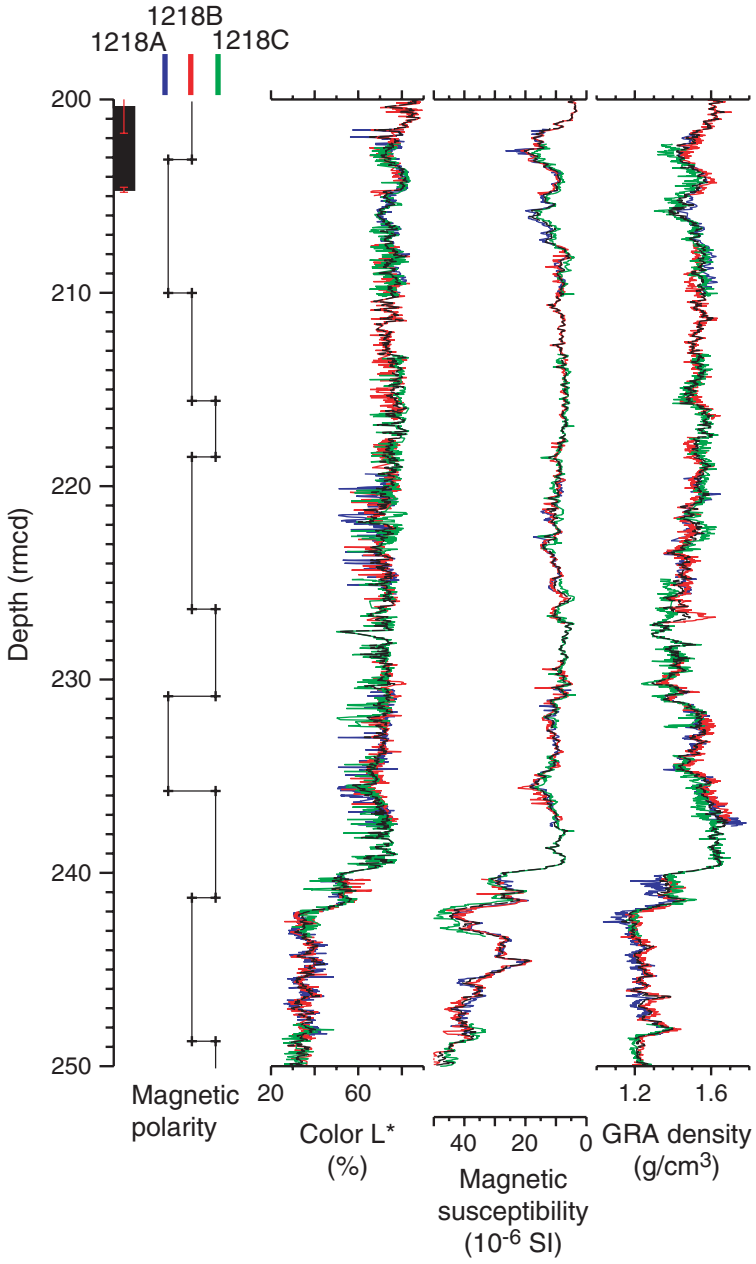

Figure F3 (continued).

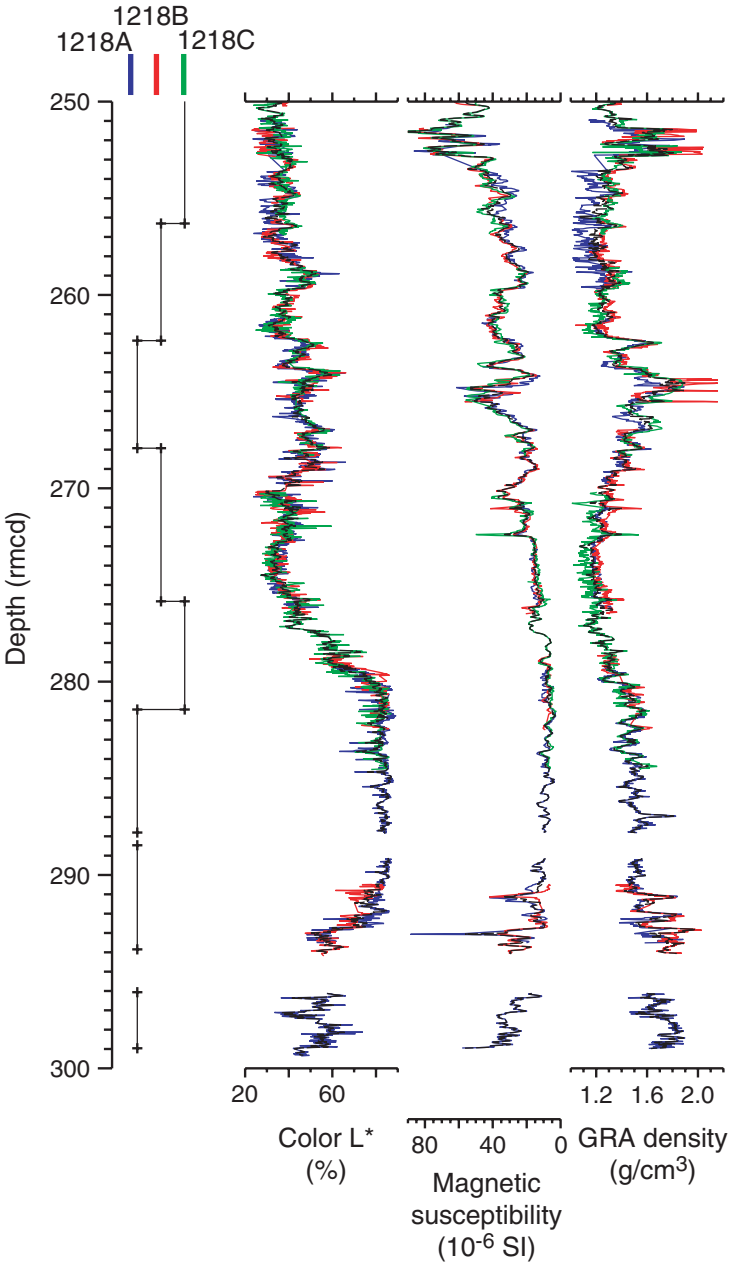

Figure F4. Site 1219 MST data on rmcd scale and stack. GRA = gamma ray attenuation. (Continued on next five pages.)

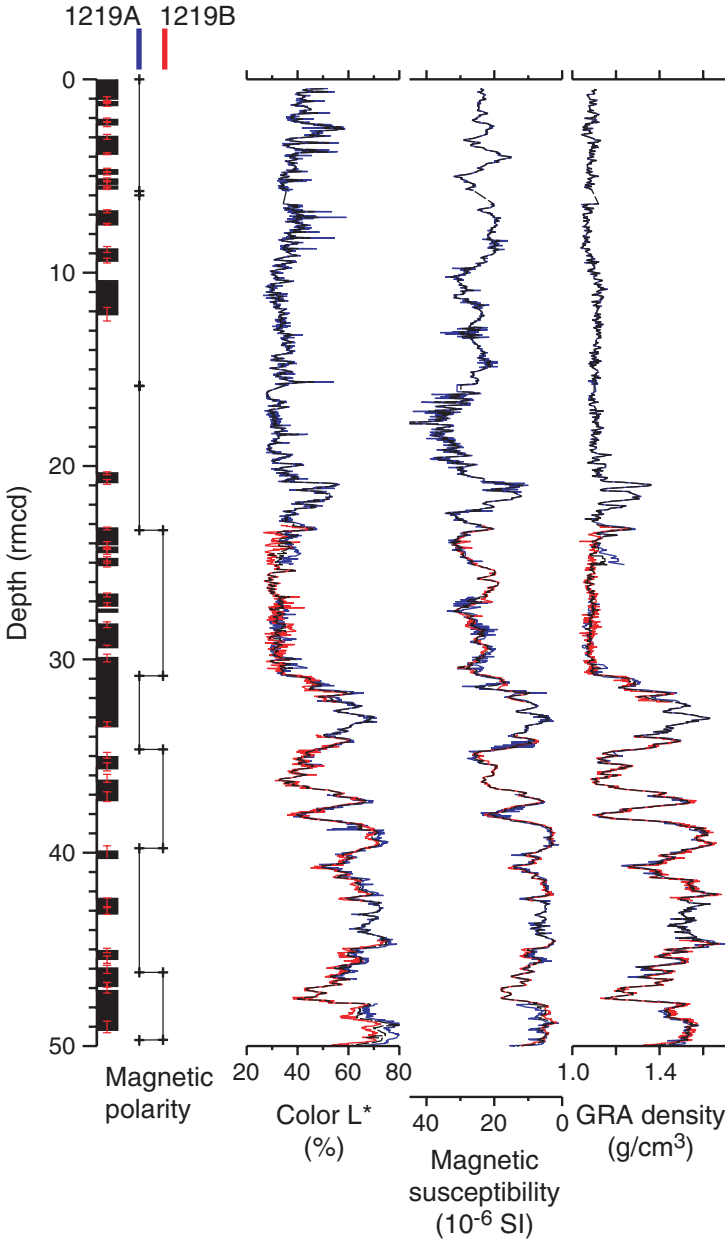

Figure F4 (continued).

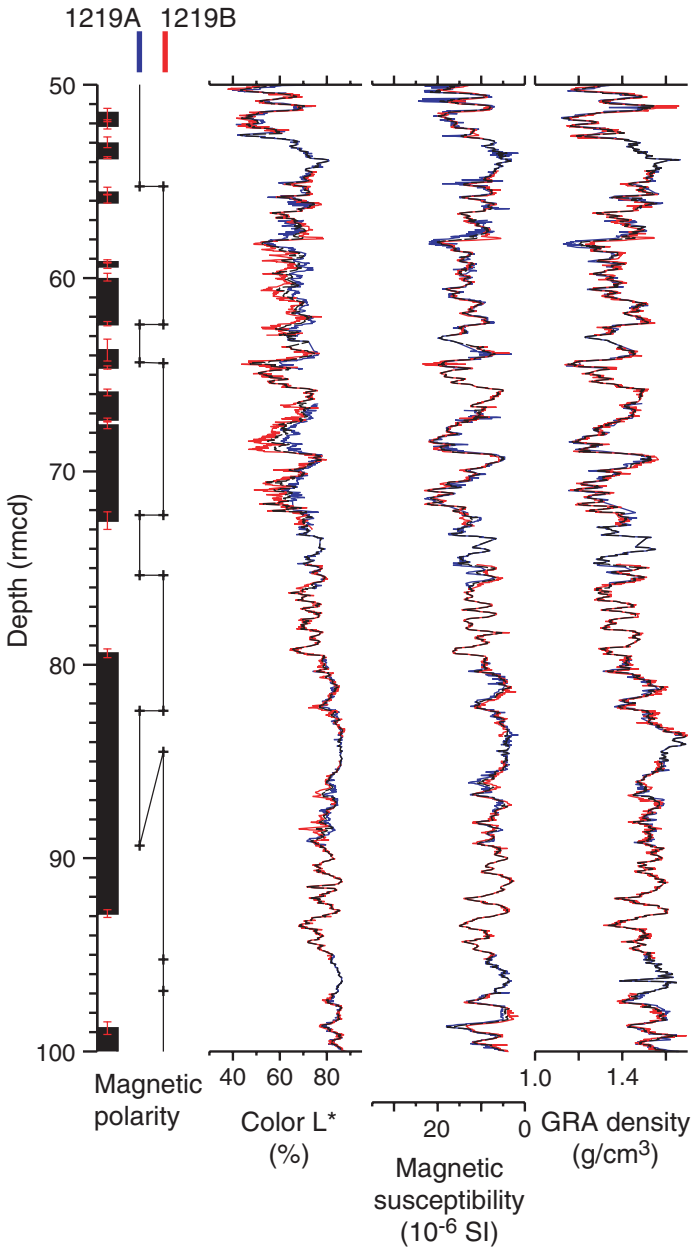

Figure F4 (continued).

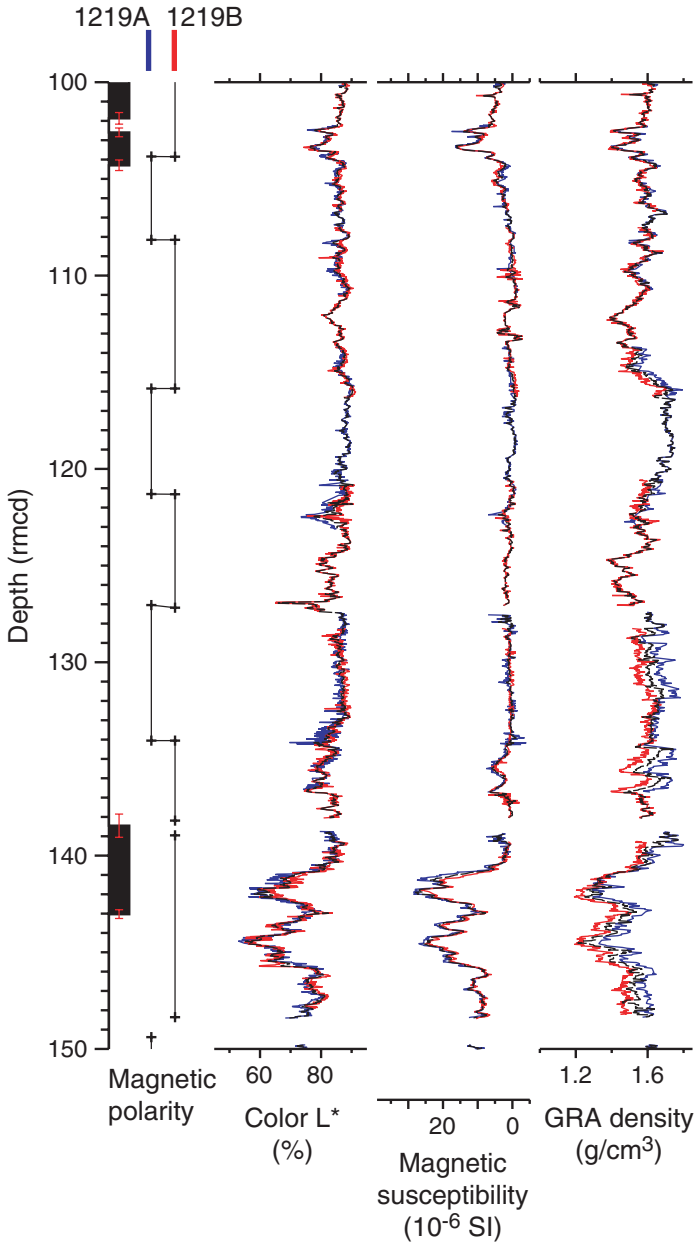

Figure F4 (continued).

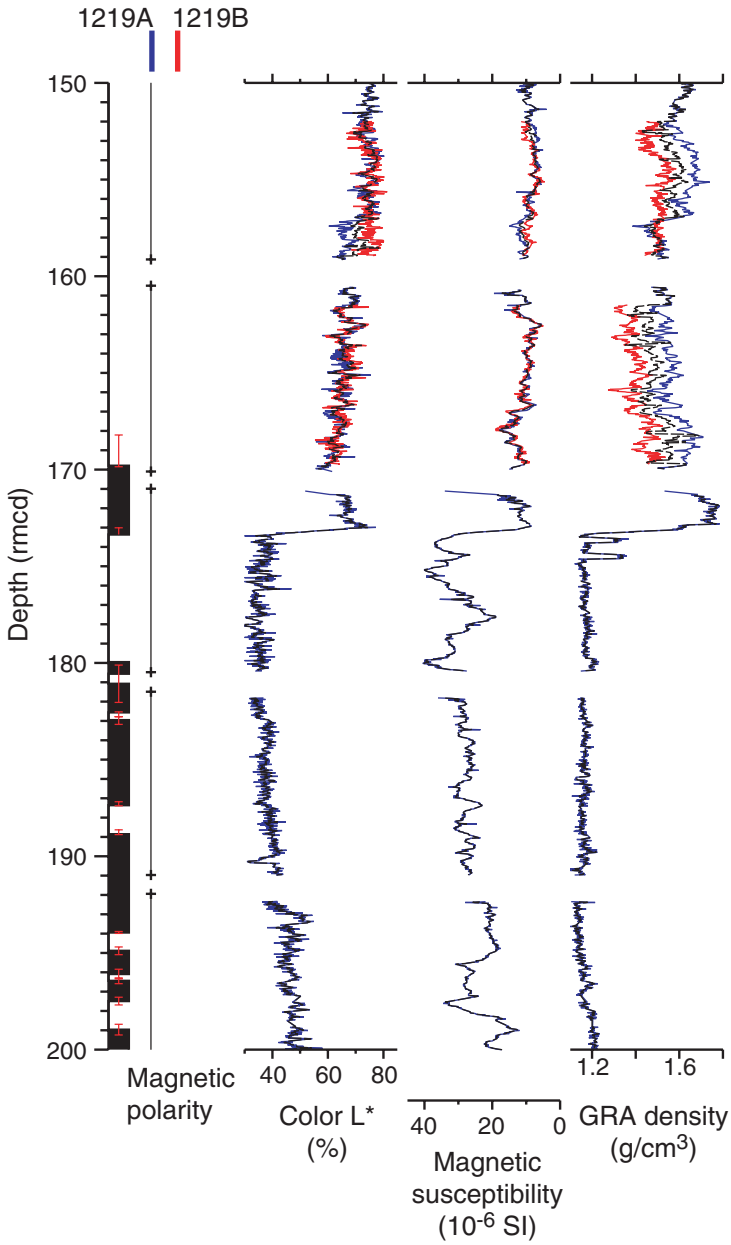

Figure F4 (continued).

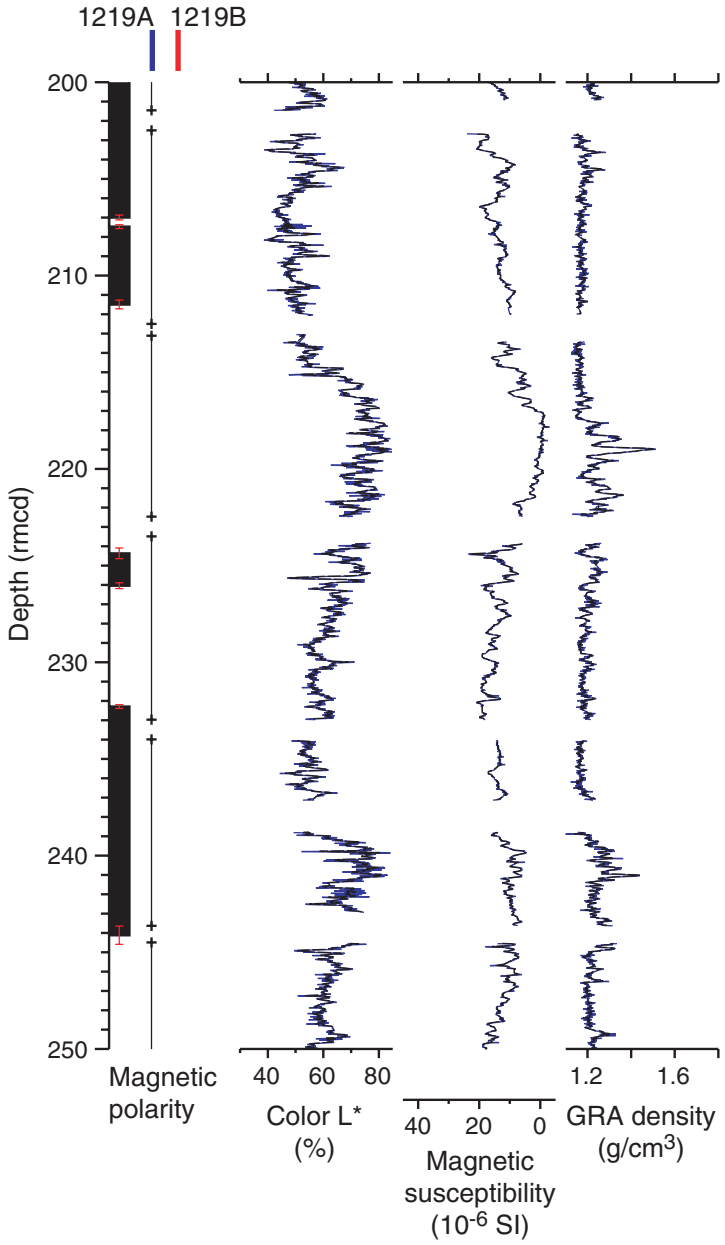

Figure F4 (continued).

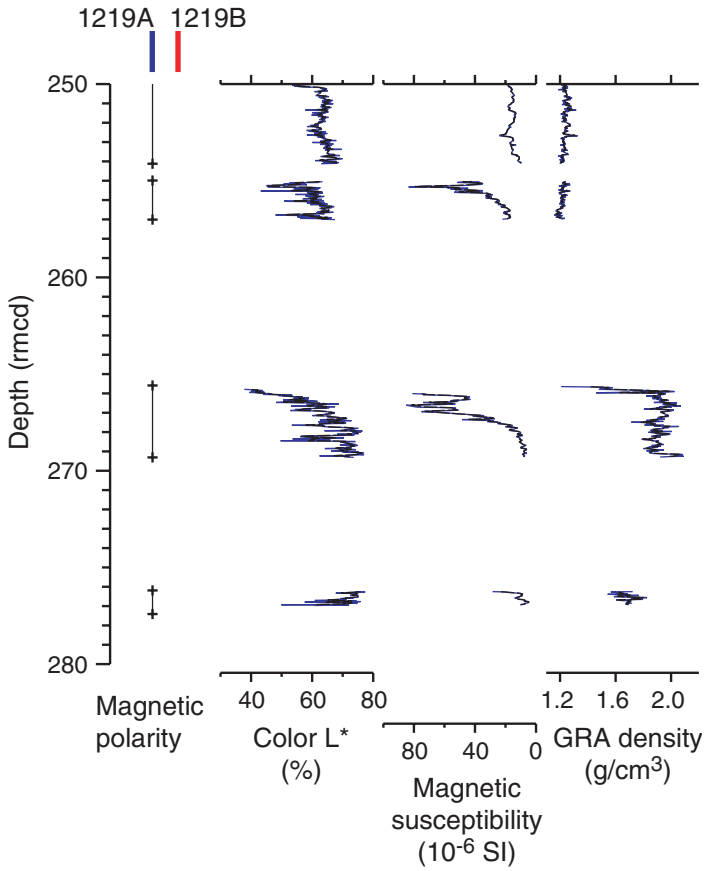

Figure F5. Site-to-site correlation of MST data (Sites 1218 and 1219). GRA = gamma ray attenuation.

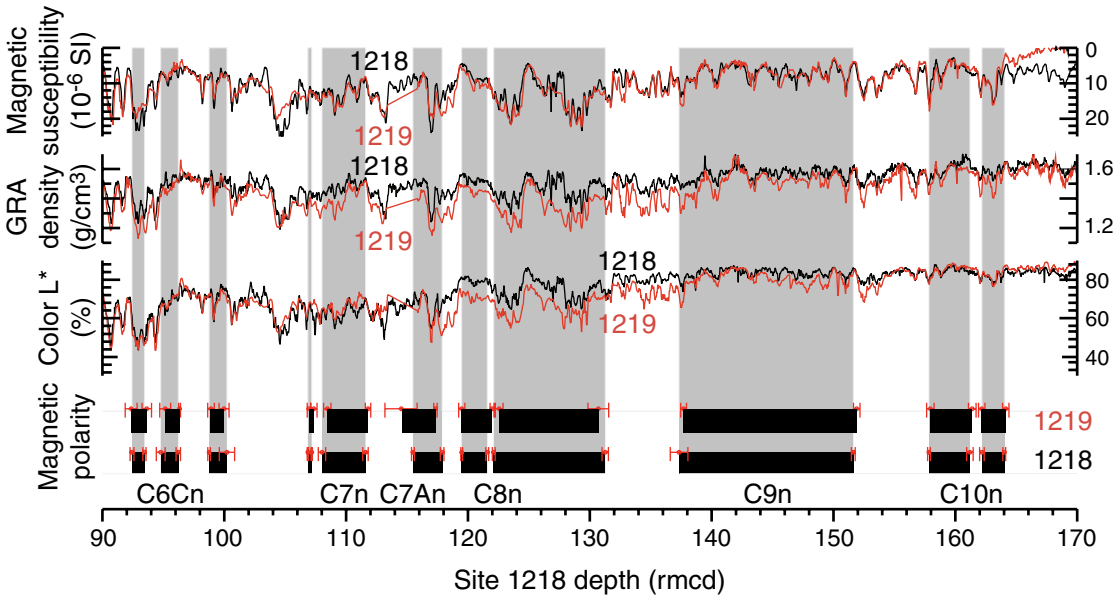

Figure F6. Estimated $CaCO_3$ content regressions from stacked MST data for Sites 1218 and 1219, compared with subsidence estimates, and shown against rmcd and the timescale of Cande and Kent (1995). MST = multisensor track, CCD = carbonate compensation depth.

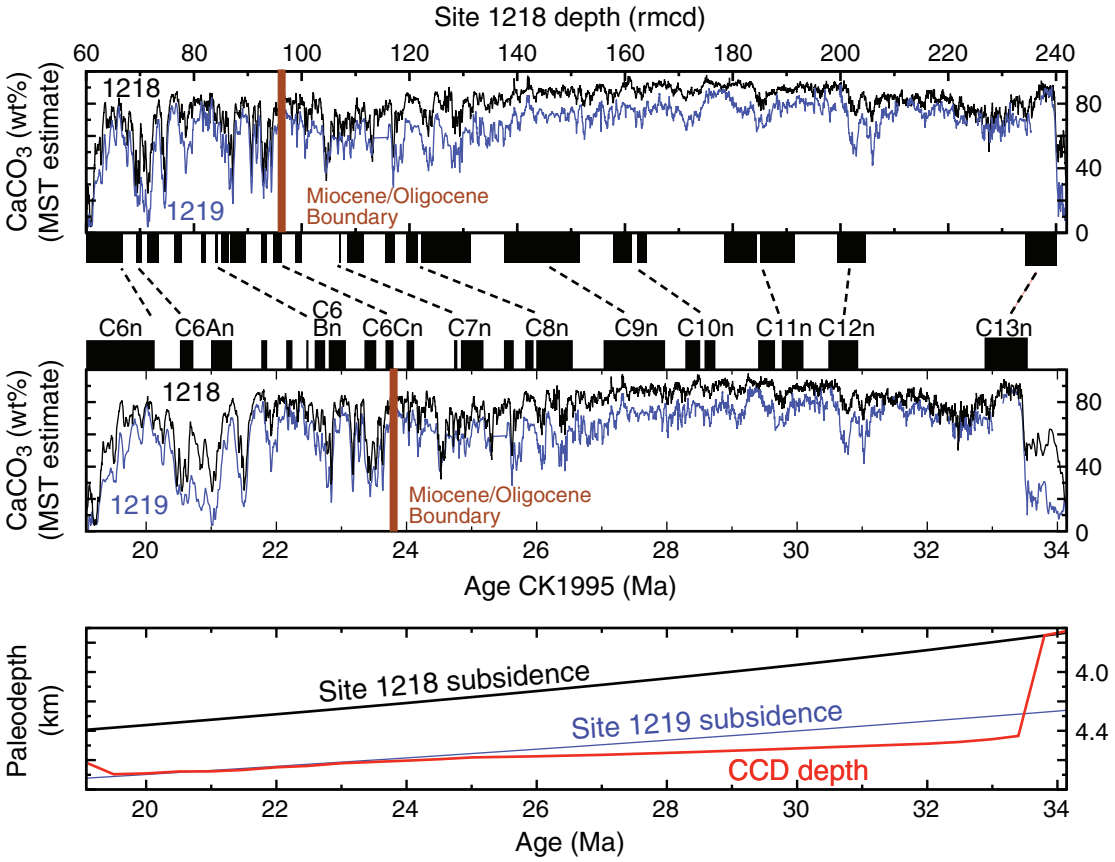

Figure F7. Stacked gamma ray attenuation (GRA) bulk density data for Sites 1218 and 1219, adjusted to wireline logging depth scale (lmbsf). GRA = gamma ray attenuation, FMS = Formation Microscanner, uncal. = uncalibrated.

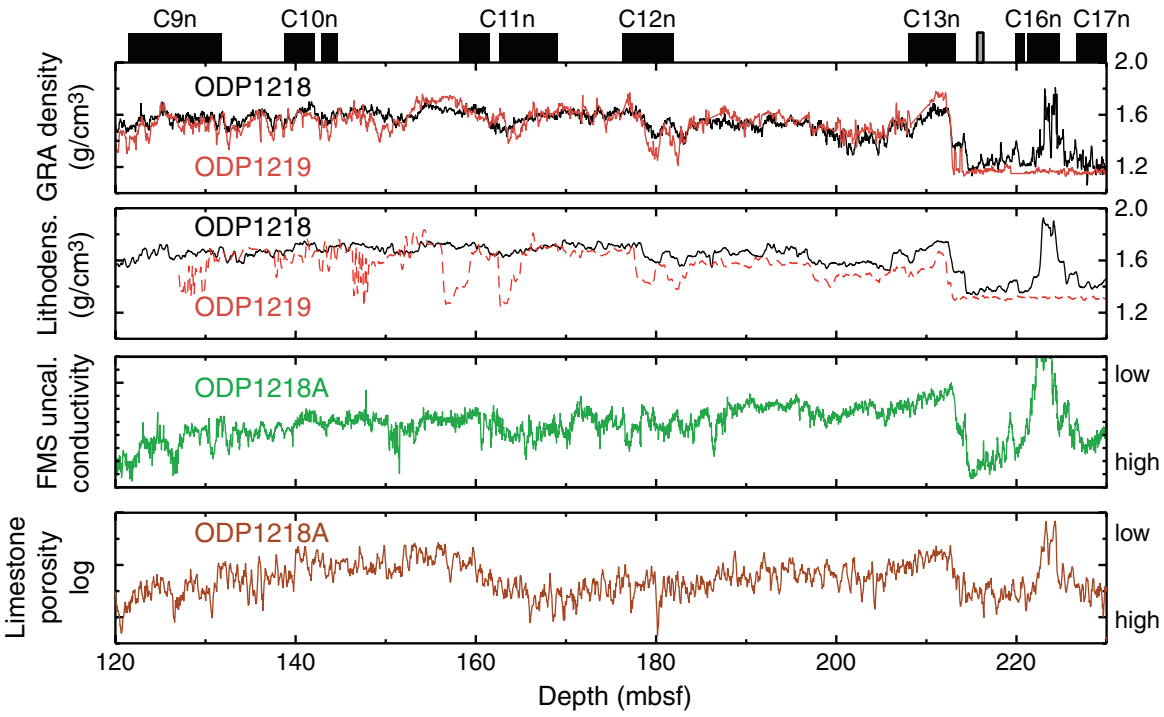

Table T1. Revised composite depth scale for Site 1218. (See table notes. Continued on next two pages.)

Core	Depth (mbsf)	Depth (mcd)	Depth (rmcd)	SPL
199-1218A-				
1H	0.00	0.00	0.00	TS
1H	6.54	6.54	6.54	S
1H	7.28	7.28	7.35	
1H	8.26	8.26	8.26	B
2H	8.20	8.98	9.35	T
2H	8.58	9.36	9.78	
2H	9.36	10.14	10.28	
2H	10.24	11.02	10.94	
2H	10.68	11.46	11.46	S
2H	17.26	18.04	18.04	S
2H	18.00	18.78	18.70	B
3H	17.70	20.04	20.04	T
3H	18.40	20.74	20.77	
3H	18.84	21.18	21.24	
3H	21.00	23.34	23.34	S
3H	26.52	28.86	28.86	S
3H	26.70	29.04	29.28	
3H	27.81	30.15	30.45	B
4H	27.20	31.62	31.35	T
4H	29.36	33.78	33.78	S
4H	36.02	40.44	40.44	S
4H	37.08	41.50	41.15	B
5H	36.70	41.50	41.75	T
5H	37.52	42.32	42.69	
5H	39.70	44.50	44.50	S
5H	45.90	50.70	50.70	S
5H	46.40	51.20	51.20	B
6H	46.20	53.04	52.92	T
6H	47.82	54.66	54.66	S
6H	54.58	61.42	61.42	S
6H	55.37	62.21	62.41	B
7H	55.70	63.76	63.46	T
7H	57.14	65.20	65.20	S
7H	63.28	71.34	71.34	S
7H	65.75	73.81	74.01	B
8H	65.20	73.16	73.16	T
8H	68.09	76.05	76.05	S
8H	72.32	80.28	80.28	S
8H	74.18	82.14	82.30	B
9H	74.70	84.96	84.96	T
9H	77.16	87.42	87.42	S
9H	83.32	93.58	93.58	S
9H	84.73	94.99	95.09	B
10H	84.20	96.10	96.00	T
10H	87.56	99.46	99.46	S
10H	92.62	104.52	104.52	S
10H	93.91	105.81	105.56	B
11H	93.70	107.10	106.72	T
11H	94.84	108.24	107.95	
11H	95.54	108.94	108.94	
11H	97.42	110.82	110.72	
11H	98.06	111.46	111.33	
11H	98.32	111.72	111.72	S
11H	102.56	115.96	115.96	S
11H	103.77	117.17	117.17	B
12H	103.20	117.67	117.67	T
12H	107.11	121.58	121.58	S
12H	110.32	124.79	124.79	S
12H	111.22	125.69	125.91	
12H	112.86	127.33	127.41	B
13H	112.70	127.61	127.51	T
13H	113.14	128.05	128.39	
13H	113.34	128.25	128.60	
13H	113.72	128.63	128.95	
13H	114.59	129.47	129.77	
13H	116.92	131.83	131.83	S
13H	120.64	135.55	135.55	S
13H	122.81	137.72	137.57	B
14H	122.20	137.62	137.77	T
14H	124.10	139.52	139.52	S
14H	130.74	146.16	146.16	S
14H	131.77	147.19	147.19	B
15H	131.70	147.92	147.92	T
15H	133.90	150.12	150.12	S
15H	141.18	157.40	157.40	S
15H	141.87	158.09	158.09	B
16H	141.20	159.04	158.74	T
16H	144.26	162.10	161.91	
16H	145.48	163.32	163.32	S
16H	149.34	167.18	167.18	S
16H	150.83	168.67	168.67	B
17H	150.70	168.60	168.60	T
17H	157.10	175.00	173.96	
17H	160.84	178.74	177.68	B
18H	160.20	180.76	180.02	T
18H	161.25	181.81	181.17	
18H	162.00	182.56	181.96	
18H	162.64	183.20	183.20	S
18H	166.20	186.76	186.76	S
18H	167.51	188.07	188.08	
18H	169.71	190.27	190.02	B
19H	169.70	190.08	190.08	T
19H	170.68	191.06	191.06	S
19H	177.96	198.34	198.34	S
19H	178.36	198.74	198.52	
19H	179.83	200.21	199.60	B
20H	179.20	201.48	201.48	T
20H	180.72	203.00	203.00	S
20H	187.62	209.90	209.90	S
20H	188.52	210.80	210.80	B
21X	NA	NA	NA	
22X	195.90	218.20	218.40	T
22X	197.34	219.64	219.72	
22X	202.26	224.56	224.58	
22X	203.63	225.93	225.72	B
23X	205.50	228.74	229.04	T
23X	206.36	229.60	230.16	
23X	206.90	230.14	230.38	
23X	207.52	230.76	230.76	S
23X	212.42	235.66	235.66	S
23X	212.88	236.12	236.12	
23X	215.39	238.63	238.63	B
24X	215.10	240.18	240.05	T
24X	215.64	240.72	240.72	
24X	216.02	241.10	241.16	
24X	216.42	241.50	241.50	
24X	216.70	241.78	241.80	
24X	217.60	242.68	242.60	
24X	218.19	243.27	243.00	
24X	220.06	245.14	244.58	
24X	221.46	246.54	245.84	
24X	223.28	248.36	247.30	
24X	223.86	248.94	247.84	
24X	224.92	250.00	248.75	B
25X	224.70	250.97	250.87	T
25X	225.39	251.66	251.65	
25X	225.91	252.18	252.17	
25X	226.12	252.39	252.27	
25X	226.30	252.57	252.56	
25X	226.48	252.75	252.65	
25X	226.68	252.95	252.77	
25X	227.78	253.93	253.75	
25X	228.54	254.61	254.60	
25X	229.00	255.13	255.33	
25X	230.12	256.39	256.45	
25X	232.60	258.87	258.74	
25X	234.31	260.58	260.48	B
26X	234.30	260.37	260.95	T
26X	236.30	262.37	262.37	S
26X	241.86	267.93	267.93	S
26X	243.16	269.23	269.15	
26X	244.17	270.24	270.24	B
27X	243.90	270.03	270.23	T
27X	246.30	272.43	272.43	
27X	250.43	276.56	276.56	B
28X	253.50	277.43	279.05	T
28X	254.90	278.83	280.03	
28X	255.68	279.61	280.51	
28X	256.38	280.31	281.45	NS
28X	262.98	286.91	288.05	B
29X	263.10	287.33	288.47	TS
29X	268.92	293.15	294.29	B
30X	270.70	294.93	296.07	TS
30X	274.34	298.57	299.71	B
199-1218B-				
1H	0.00	0.00	0.07	T
1H	0.56	0.56	0.66	
1H	1.96	1.96	1.81	
1H	2.34	2.34	2.26	
1H	2.82	2.82	2.70	
1H	3.50	3.50	3.62	
1H	3.86	3.86	3.98	B
2H	3.90	5.30	5.20	T
2H	4.69	5.96	6.15	
2H	5.38	6.54	6.54	S
2H	10.30	11.46	11.46	S
2H	11.14	12.30	12.42	
2H	11.28	12.44	12.54	
2H	11.34	12.50	12.70	
2H	12.73	13.89	14.12	B
3H	13.40	17.22	16.84	T
3H	13.84	17.66	17.64	
3H	14.22	18.04	18.04	S
3H	19.52	23.34	23.34	S
3H	20.82	24.64	24.75	
3H	23.39	27.21	27.36	B
4H	22.90	28.08	28.08	T
4H	23.68	28.86	28.86	S
4H	28.60	33.78	33.78	S
4H	28.96	34.14	34.24	
4H	31.60	36.78	36.38	B
5H	32.40	38.06	38.06	T
5H	34.78	40.44	40.44	S
5H	38.84	44.50	44.50	S
5H	39.40	45.06	45.06	
5H	42.42	48.08	48.38	B
6H	41.90	49.56	49.36	T
6H	43.04	50.70	50.70	S
6H	47.00	54.66	54.66	S
6H	49.63	57.29	57.29	
6H	51.02	58.68	58.65	B
7H	51.40	58.69	58.99	T
7H	54.13	61.42	61.42	S
7H	57.91	65.20	65.20	S
7H	58.20	65.49	65.56	
7H	61.27	68.56	68.26	B
8H	60.90	69.29	69.29	T
8H	62.95	71.34	71.34	S
8H	67.66	76.05	76.05	S
8H	70.28	78.67	78.47	B
9H	70.40	78.74	78.74	T
9H	71.94	80.28	80.28	S
9H	79.08	87.42	87.42	S
9H	79.66	88.00	87.80	
9H	80.47	88.81	88.81	B
10H	79.90	90.70	90.40	T

Table T1 (continued).

Core	Depth (mbsf)	Depth (mcd)	Depth (rmcd)	SPL
10H	80.22	91.02	91.29	
10H	82.78	93.58	93.58	S
10H	88.66	99.46	99.46	S
10H	89.68	100.48	100.48	B
11H	89.40	102.78	102.68	T
11H	91.14	104.52	104.52	S
11H	98.34	111.72	111.72	S
11H	99.41	112.79	112.90	B
12H	98.90	114.14	113.84	T
12H	99.94	115.18	115.15	
12H	100.72	115.96	115.96	S
12H	106.34	121.58	121.58	S
12H	109.07	124.31	124.01	B
13H	108.40	123.89	124.02	T
13H	109.30	124.79	124.79	S
13H	116.34	131.83	131.83	S
13H	118.51	134.00	134.00	B
14H	117.90	134.36	134.36	T
14H	119.09	135.55	135.55	S
14H	123.06	139.52	139.52	S
14H	127.76	144.22	144.48	B
15H	127.40	145.22	145.02	T
15H	128.34	146.16	146.16	S
15H	132.30	150.12	150.12	S
15H	135.60	153.42	153.62	
15H	137.41	155.23	155.23	B
16H	136.90	155.92	155.92	T
16H	138.38	157.40	157.40	S
16H	144.30	163.32	163.32	S
16H	145.92	164.94	164.74	B
17H	146.40	166.18	166.18	T
17H	147.40	167.18	167.18	S
17H	154.36	174.14	174.14	S
17H	156.41	176.19	176.19	B
18H	155.90	176.02	176.22	T
18H	159.08	179.20	179.20	S
18H	163.08	183.20	183.20	S
18H	164.56	184.68	184.96	
18H	165.91	186.03	186.03	B
19X	165.40	184.44	184.79	T
19X	166.61	185.65	185.76	
19X	166.99	186.03	186.39	
19X	169.43	188.47	188.00	
19X	172.83	191.87	191.85	
19X	175.20	194.24	194.24	B
20X	175.10	195.80	195.96	T
20X	175.95	196.65	196.68	
20X	177.64	198.34	198.34	S
20X	182.30	203.00	203.00	S
20X	183.71	204.41	205.35	B
21X	184.80	207.32	207.32	T
21X	187.38	209.90	209.90	S
21X	192.96	215.48	215.48	S
21X	193.42	215.94	215.78	
21X	194.50	217.02	216.92	B
22X	194.40	217.42	217.42	T
22X	195.36	218.38	218.38	S
22X	203.23	226.25	226.25	S
22X	203.99	227.01	227.26	B
23X	204.10	227.88	228.82	T
23X	205.48	229.34	230.26	
23X	206.20	230.10	230.72	
23X	206.99	230.89	231.43	
23X	208.34	232.22	232.44	
23X	209.65	233.51	233.72	
23X	210.00	233.85	233.95	
23X	211.88	235.70	235.73	
23X	212.68	236.48	236.35	
23X	213.02	236.81	236.87	
23X	213.82	237.60	237.60	B
24X	213.70	240.16	240.21	T
24X	214.20	240.66	240.73	
24X	214.72	241.18	241.18	S
24X	222.14	248.60	248.60	S
24X	222.36	248.82	249.23	
24X	222.60	249.06	249.77	
24X	223.46	249.92	250.50	B
25X	223.30	251.43	251.05	T
25X	223.78	251.91	251.78	
25X	224.24	252.37	252.25	
25X	224.61	252.74	252.57	
25X	224.72	252.85	252.75	
25X	227.60	255.73	255.63	B
26X	228.30	255.91	255.91	T
26X	228.70	256.31	256.31	S
26X	234.76	262.37	262.37	S
26X	235.88	263.49	263.71	
26X	237.89	265.50	265.80	B
27X	237.90	267.03	266.80	T
27X	238.80	267.93	267.93	S
27X	246.72	275.85	275.85	S
27X	247.65	276.78	276.78	B
28X	247.50	278.03	278.03	T
28X	249.20	279.73	279.65	
28X	249.80	280.33	280.32	
28X	250.90	281.43	281.27	
28X	252.67	283.20	283.40	B
29X	257.20	287.83	290.33	T
29X	258.52	289.15	291.27	
29X	258.82	289.45	291.97	
29X	259.74	290.37	292.71	
29X	261.64	292.27	294.57	B
199-1218C-				
1H	55.00	63.04	62.84	T
1H	57.46	65.50	65.66	
1H	59.42	67.46	67.60	
1H	61.36	69.40	69.49	
1H	64.96	73.00	73.25	B
2H	64.50	73.86	73.65	T
2H	65.30	74.66	74.66	
2H	68.92	78.28	78.46	
2H	71.56	80.92	81.36	
2H	74.03	83.39	83.64	B
3H	74.00	83.78	83.65	T
3H	74.95	84.73	84.73	
3H	77.40	87.18	87.28	
3H	80.94	90.72	90.71	
3H	84.16	93.94	93.54	B
4H	83.50	95.08	94.83	T
4H	87.54	99.12	99.12	
4H	92.18	103.76	104.40	B
5H	93.00	105.82	105.75	T
5H	94.75	107.59	107.47	
5H	98.64	111.44	111.61	
5H	100.17	112.97	113.44	
5H	101.35	114.16	114.86	
5H	103.13	115.95	116.95	B
6H	102.50	118.08	118.08	T
6H	105.40	120.98	121.73	
6H	107.10	122.68	123.02	
6H	107.82	123.40	123.88	
6H	112.24	127.82	127.60	B
7H	112.00	126.09	127.00	T
7H	113.89	127.98	127.90	
7H	114.00	128.09	128.25	
7H	114.40	128.49	128.57	
7H	115.90	129.99	130.01	
7H	117.96	132.05	131.86	
7H	119.24	133.33	132.95	
7H	122.21	136.30	135.90	B
8H	121.50	135.97	135.97	T
8H	124.92	139.39	139.43	
8H	127.28	141.75	141.96	
8H	128.53	143.00	143.39	
8H	131.27	145.74	145.74	B
9H	131.00	146.90	147.20	T
9H	135.10	151.00	150.95	
9H	138.90	154.80	154.60	
9H	141.08	156.98	156.98	B
10H	144.50	162.34	162.34	T
10H	145.60	163.44	163.44	
10H	150.30	168.14	167.80	
10H	154.26	172.10	171.60	B
11H	154.00	172.62	172.62	T
11H	155.52	174.14	174.14	S
11H	160.58	179.20	179.20	S
11H	163.99	182.61	183.06	B
12X	163.50	183.28	183.85	T
12X	164.78	184.56	184.79	
12X	166.27	185.05	186.04	
12X	166.98	186.76	186.76	S
12X	171.28	191.06	191.06	S
12X	172.23	192.01	192.01	B
13X	172.00	191.76	191.76	T
13X	178.58	198.34	198.34	
13X	178.97	198.73	198.50	
13X	179.81	199.57	199.10	
13X	180.09	199.85	199.30	
13X	181.33	201.09	199.99	B
14X	181.60	201.41	202.21	T
14X	186.92	206.73	206.73	
14X	191.18	210.99	210.99	B
15X	191.20	213.12	213.12	T
15X	192.54	214.46	214.46	
15X	193.22	215.14	214.92	
15X	193.56	215.48	215.48	S
15X	196.46	218.38	218.38	S
15X	198.60	220.52	220.94	
15X	199.28	221.20	222.16	
15X	199.66	221.58	222.62	
15X	200.99	222.91	223.79	B
16X	200.80	224.70	224.40	T
16X	202.18	226.08	225.90	
16X	202.35	226.25	226.25	S
16X	206.86	230.76	230.76	S
16X	207.86	231.76	231.88	
16X	209.34	233.24	233.24	B
17X	210.40	233.86	233.86	T
17X	212.20	235.66	235.66	S
17X	217.72	241.18	241.18	S
17X	218.12	241.58	241.50	
17X	218.50	241.96	241.91	
17X	219.40	242.86	242.92	
17X	220.12	243.58	243.66	B
18X	223.00	247.42	247.52	T
18X	224.18	248.60	248.60	S
18X	231.89	256.31	256.31	S
18X	232.74	257.16	257.16	B
19X	232.60	257.53	258.48	T
19X	234.22	259.15	259.69	
19X	235.36	260.29	260.78	
19X	236.15	261.08	261.18	
19X	237.58	262.51	262.51	
19X	238.84	263.78	263.88	
19X	239.68	264.62	264.90	
19X	240.42	265.36	266.16	
19X	240.82	265.76	267.00	

Table T1 (continued).

Core	Depth (mbsf)	Depth (mcd)	Depth (rmcd)	SPL
19X	242.20	267.13	268.75	B
20X	242.20	269.65	269.45	T
20X	244.98	272.43	272.48	
20X	247.73	275.18	275.18	B
21X	247.20	274.77	274.77	T
21X	248.28	275.85	275.85	S
21X	253.88	281.45	281.45	NS
21X	254.34	281.91	282.15	
21X	255.30	282.87	283.65	
21X	256.68	284.25	285.33	B

Notes: mbsf = meters below seafloor, mcd = meters composite depth, rmcd = revised meters composite depth. The SPL column indicates whether a particular tie-point corresponds to a splice point (S), to modified splice points (NS), or to the top (T) or bottom (B) of a core. NA = not available. This table is also available in **ASCII.**

Table T2. Revised composite depth scale for Site 1219. [N1]

Core	Depth (mbsf)	Depth (mcd)	Depth (rmcd)	SPL
199-1219A-				
1H	0.00	0.00	0.00	TS
1H	5.95	5.95	5.95	BS
2H	6.00	6.00	6.00	TS
2H	15.78	15.66	15.78	S
2H	16.04	16.04	16.04	B
3H	15.50	15.50	15.50	T
3H	15.78	15.66	15.78	S
3H	23.32	23.32	23.32	S
3H	25.35	25.35	25.50	B
4H	25.00	25.88	25.88	T
4H	29.97	30.85	30.85	S
4H	33.78	34.66	34.66	S
4H	34.87	35.75	35.75	B
5H	34.50	36.79	36.79	T
5H	37.48	39.77	39.77	S
5H	43.90	46.19	46.19	S
5H	44.47	46.76	46.76	B
6H	44.00	48.02	47.58	T
6H	45.49	49.33	49.51	S
6H	51.24	55.26	55.26	S
6H	52.15	56.17	56.17	
6H	53.95	57.97	57.57	B
7H	53.50	55.57	55.87	T
7H	55.56	57.63	58.00	
7H	56.82	58.89	58.60	
7H	57.44	59.51	59.30	
7H	60.33	62.40	62.40	S
7H	62.12	63.98	64.19	S
7H	62.99	65.06	65.06	B
8H	63.00	66.05	66.05	T
8H	69.21	72.26	72.26	S
8H	72.32	75.37	75.37	S
8H	73.09	76.14	76.45	B
9H	72.50	79.87	79.32	T
9H	75.01	82.38	82.38	S
9H	81.98	89.35	89.35	S
9H	82.39	89.76	89.76	B
10H	82.00	90.97	91.77	T
10H	89.32	98.29	99.09	NS?
10H	91.62	100.59	100.80	B
11H	91.50	104.91	102.07	T
11H	92.98	106.08	103.55	S
11H	97.58	110.99	108.15	S
11H	101.19	114.60	111.76	B
12H	101.00	116.13	113.29	T
12H	103.55	118.68	115.84	S
12H	108.78	123.65	121.07	S
12H	111.14	126.27	123.43	B
13H	110.50	130.31	127.25	TS
13H	117.30	136.89	134.05	S
13H	118.16	137.75	135.10	
13H	120.13	139.72	136.88	B
14H	120.00	141.45	138.61	T
14H	127.08	148.53	145.53	
14H	130.01	151.46	148.62	B
15H	129.50	152.49	149.51	TS
15H	139.27	162.12	159.28	BS
16H	139.00	163.33	160.49	TS
16H	148.94	173.27	170.43	BS
17H	148.50	173.83	170.99	TS
17H	158.33	183.66	180.82	BS
18H	158.00	184.33	181.49	TS
18H	168.02	194.35	191.51	BS
19H	167.50	194.89	191.99	TS
19H	177.01	204.34	201.50	BS
20H	177.00	205.33	202.49	TS
20H	186.93	215.26	212.42	BS
21H	186.50	215.71	212.99	TS
21H	196.35	225.68	222.84	BS
22H	196.00	226.33	223.49	TS
22H	205.84	236.17	233.33	BS
23H	205.50	236.83	233.99	TS
23H	215.47	246.80	243.96	BS
24H	215.00	247.33	244.49	TS
24H	224.91	257.24	254.40	BS
25X	224.50	257.83	254.99	TS
25X	226.95	260.28	257.44	BS
26X	234.10	268.43	265.59	TS
26X	238.10	272.43	269.59	BS
27X	243.70	279.03	276.19	TS
27X	244.92	280.25	277.41	BS
199-1219B-				
2H	21.00	22.56	22.56	T
2H	21.76	23.32	23.32	S
2H	29.29	30.85	30.85	S
2H	30.95	32.51	32.51	B
3H	30.50	33.85	33.85	T
3H	31.31	34.66	34.66	S
3H	36.42	39.77	39.77	S
3H	36.84	40.19	40.19	
3H	39.68	43.03	42.73	B
4H	40.00	44.41	44.41	T
4H	41.78	46.19	46.19	S
4H	45.10	49.33	49.51	S
4H	46.52	50.82	50.93	
4H	48.75	53.16	52.86	B
5H	49.50	54.40	54.40	T
5H	50.36	55.26	55.26	S
5H	57.50	62.40	62.40	S
5H	58.79	63.69	63.39	B
6H	59.00	63.34	63.34	T
6H	59.85	63.98	64.19	S
6H	67.92	72.26	72.26	S
6H	68.97	73.31	73.31	B
7H	68.50	74.48	74.48	T
7H	69.39	75.37	75.37	S
7H	76.40	82.38	82.38	S
7H	78.30	84.28	84.00	B
8H	78.00	89.91	84.50	TS
8H	78.84	90.75	85.61	
8H	79.42	91.33	86.79	
8H	80.84	92.75	88.26	
8H	88.10	100.01	95.52	BS
9H	87.50	100.11	96.87	TS
9H	88.92	101.46	98.69	
9H	92.82	105.17	102.59	
9H	93.78	106.08	103.55	S
9H	97.00	109.61	106.97	B
10H	97.00	110.20	107.36	T
10H	97.79	110.99	108.15	S
10H	105.48	118.68	115.84	S
10H	106.81	120.01	117.17	B
11H	106.50	120.57	117.73	T
11H	109.84	123.65	121.07	S
11H	116.14	130.42	127.37	S
11H	116.38	130.45	127.61	B
12H	116.00	131.29	128.20	T
12H	121.60	136.89	134.05	S
12H	125.74	141.03	138.19	S
12H	125.88	141.17	138.33	B
13H	125.50	141.79	138.95	T
13H	125.50	141.79	138.95	S
13H	134.98	151.34	148.43	S
13H	135.18	151.47	148.63	B
14H	135.00	152.29	150.00	T
14H	140.24	157.53	154.69	
14H	145.13	162.42	159.58	B
15H	144.50	163.85	160.85	T
15H	149.98	169.33	166.49	
15H	153.18	172.53	169.99	B
16H	154.00	173.35	170.81	T
16H	157.95	177.30	174.76	B

Notes: mbsf = meters below seafloor, mcd = meters composite depth, rmcd = revised meters composite depth. The SPL column indicates whether a particular tie-point corresponds to a splice point (S), to modified splice points (NS), or to the top (T) or bottom (B) of a core. This table is also available in ASCII.

Table T3. Stacked multisensor track data from Site 1218 (on 1218 rmcd depth scale).

Depth (rmcd)	GRA stack (g/cm³)	MS stack (10^{-6} SI)	Color reflectance stack (%)		
			L*	a*	b*
0.42	1.090	19.4	52.65	7.11	20.86
0.44	1.067	20.0	51.83	6.76	20.25
0.46	1.091	20.5	51.49	6.46	19.74
0.48	1.114	20.7	52.01	6.50	19.83
0.50	1.098	20.5	53.26	7.15	20.91
0.52	1.081	20.4	53.90	7.47	21.41
0.54	1.092	21.0	54.21	7.31	20.91
0.56	1.104	22.0	54.50	7.18	20.31
0.58	1.103	22.4	54.60	7.19	20.41
0.60	1.100	22.2	54.36	7.27	20.61
0.62	NA	21.7	53.58	7.16	20.34
0.64	1.079	18.4	52.90	7.09	20.26
0.66	NA	18.5	53.31	7.25	20.60
0.68	1.058	19.8	53.72	7.46	20.59
0.70	1.054	21.3	54.34	7.45	20.14
0.72	1.053	22.1	54.59	7.29	20.02
0.74	1.078	22.1	54.19	7.16	20.16
0.76	1.104	22.3	54.11	7.14	20.25
0.78	1.107	22.7	54.62	7.16	20.10
0.80	1.107	23.0	54.62	7.04	19.77
0.82	1.111	23.0	54.23	6.97	19.75
0.84	1.116	23.1	53.96	7.07	20.24
0.86	1.114	23.2	53.60	7.26	20.78
0.88	1.111	23.0	53.44	7.39	20.88
0.90	1.092	22.6	53.48	7.30	20.76
0.92	1.074	22.4	53.63	7.14	20.64
0.94	1.090	22.3	53.21	7.02	20.39
0.96	1.108	22.5	53.13	6.96	20.14
0.98	1.124	22.7	53.76	7.07	20.17
1.00	1.138	22.6	54.20	7.07	20.04
1.02	1.117	22.2	54.15	6.83	19.51
1.04	1.093	21.4	54.09	6.80	19.64
1.06	1.086	20.7	54.07	6.92	20.06
1.08	1.081	20.7	53.89	6.91	19.91
1.10	1.090	20.7	54.04	6.85	19.69
1.12	1.101	21.0	54.73	6.96	19.88
1.14	1.108	20.7	55.10	7.22	20.59
1.16	1.114	19.7	55.34	7.29	20.79
1.18	1.100	19.6	55.87	7.04	19.46
1.20	1.087	21.0	56.32	6.58	17.20
1.22	1.093	22.3	56.31	6.27	16.05
1.24	1.099	23.0	56.03	6.16	15.70
1.26	1.086	23.6	54.28	6.10	15.45
1.28	1.072	23.8	52.51	5.98	15.03
1.30	1.089	23.5	53.01	5.91	14.74
1.32	1.108	23.1	53.51	5.97	14.90
1.34	1.117	23.0	53.36	6.12	15.30
1.36	1.125	NA	53.89	6.28	15.63
1.38	NA	NA	53.60	6.31	15.54
1.56	NA	23.2	54.27	7.41	20.01
1.58	1.136	23.8	54.35	7.34	19.65
1.60	1.113	24.2	54.44	7.57	20.50
1.62	1.090	24.3	54.85	7.76	21.17
1.64	1.091	24.7	55.16	7.67	20.74
1.66	1.094	24.1	54.19	7.33	19.79
1.68	1.103	24.6	52.33	6.81	18.74
1.70	1.099	25.0	51.98	6.74	18.81
1.72	1.104	25.5	53.52	7.23	19.95
1.74	1.119	26.5	52.18	6.92	19.25
1.76	1.122	27.6	52.49	7.27	20.11
1.78	1.112	28.1	52.79	7.29	20.27
1.80	1.106	27.2	53.40	7.38	20.52
1.82	1.107	26.6	53.76	7.50	20.86
1.84	1.110	26.8	53.07	7.36	20.63
1.86	1.113	27.3	52.56	7.02	19.97
1.88	1.108	27.2	53.26	7.09	20.12
1.90	1.103	26.4	54.02	7.44	21.03
1.92	1.102	25.4	54.23	7.66	21.48
1.94	1.101	24.8	54.26	7.66	21.41
1.96	1.099	24.6	53.49	7.48	20.92
1.98	1.100	24.6	52.08	7.18	20.11
2.00	1.102	25.1	51.70	7.05	19.81
2.02	1.101	25.9	50.95	6.79	19.31
2.04	1.108	26.2	50.35	6.43	18.40
2.06	1.123	26.5	51.63	6.52	18.27
2.08	1.131	26.9	52.61	6.86	18.97
2.10	1.123	27.1	50.84	6.52	18.53
2.12	1.119	27.4	49.30	6.01	17.67
2.14	1.120	27.3	49.93	6.04	17.87
2.16	1.121	27.1	51.05	6.23	18.06
2.18	1.119	27.0	51.86	6.30	18.05
2.20	1.119	26.3	52.71	6.43	18.42
2.22	1.117	25.3	53.56	6.59	18.81
2.24	1.099	24.3	52.93	6.40	17.96
2.26	1.079	23.6	52.22	6.35	17.37
2.28	1.088	23.9	53.26	6.79	19.04
2.30	1.097	24.3	54.31	7.28	20.59
2.32	1.101	24.6	54.58	7.43	20.84
2.34	1.102	24.4	54.53	7.52	21.13
2.36	1.097	24.1	53.50	7.54	21.39
2.38	1.100	24.4	51.75	7.19	20.85
2.40	1.111	24.9	50.33	6.51	19.42
2.42	1.110	25.7	49.49	5.93	18.03
2.44	1.106	26.3	48.16	5.54	17.14
2.46	1.111	26.7	47.19	5.27	16.65
2.48	1.118	27.2	46.52	4.89	15.66
2.50	1.125	27.6	45.63	4.69	15.16
2.52	1.123	27.6	44.61	4.59	15.00
2.54	1.111	27.6	44.31	4.51	14.66
2.56	1.113	27.7	44.70	4.61	14.92
2.58	1.127	27.4	46.09	4.97	15.92
2.60	1.124	27.2	47.46	5.35	16.90
2.62	1.113	26.9	48.41	5.73	17.72
2.64	1.110	26.8	49.63	6.25	18.60
2.66	1.106	26.8	50.87	6.61	19.07
2.68	1.111	26.6	51.44	6.66	18.97
2.70	1.119	26.3	51.30	6.65	18.91
2.72	1.116	25.9	49.61	6.12	17.79
2.74	1.113	25.9	48.68	5.71	16.86
2.76	1.114	26.1	48.48	5.63	16.56
2.78	1.117	26.4	47.61	5.54	16.20
2.80	1.118	26.6	47.13	5.36	15.28
2.82	1.116	26.3	47.06	5.42	15.32
2.84	1.108	25.7	47.39	5.44	15.54
2.86	1.105	25.5	47.95	5.23	14.96
2.88	1.094	25.2	48.83	5.10	14.54
2.90	1.093	24.7	48.55	4.89	14.25
2.92	NA	24.5	45.57	4.66	14.40
2.94	NA	NA	45.80	4.84	14.86
3.00	NA	NA	47.95	4.90	12.18
3.02	NA	26.0	45.65	3.99	9.95
3.04	1.144	26.2	43.88	4.07	10.21
3.06	1.144	26.2	46.15	4.95	13.74
3.08	1.139	26.3	47.15	4.89	13.64
3.10	1.133	26.5	46.76	4.91	13.62
3.12	1.128	26.4	45.92	4.97	13.85
3.14	1.108	26.1	46.25	4.92	13.66
3.16	1.097	26.0	46.57	4.80	13.17
3.18	1.099	25.6	46.13	4.65	12.89
3.20	1.106	25.3	45.48	4.50	12.80
3.22	1.106	25.4	44.53	4.26	12.29
3.24	1.107	25.7	43.79	4.24	12.29

Notes: GRA = gamma ray attenuation, MS = magnetic susceptibility, NA = not available. Only a portion of this table appears here. The complete table is available in **ASCII.**

Table T4. Stacked multisensor track data from Site 1219 (on 1219 rmcd depth scale).

Depth (rmcd)	GRA stack (g/cm³)	MS stack (10^{-6} SI)	Color reflectance stack (%)		
			L*	a*	b*
0.68	1.096	24.2	43.47	5.68	17.45
0.70	1.100	24.0	40.17	5.17	15.75
0.72	1.104	23.9	40.00	5.27	15.43
0.74	1.102	23.5	40.36	5.43	15.83
0.76	1.100	23.1	39.93	5.33	15.40
0.78	1.084	22.9	39.47	5.21	14.76
0.80	1.067	22.8	39.86	5.28	15.26
0.82	NA	22.9	41.33	5.37	15.75
0.84	NA	NA	42.98	5.59	16.09
0.86	NA	NA	42.64	5.38	15.59
0.88	NA	NA	42.39	5.18	15.12
0.90	NA	NA	42.84	5.28	15.42
0.92	NA	NA	NA	NA	NA
0.94	NA	NA	42.30	5.45	16.42
0.96	NA	NA	NA	NA	NA
0.98	NA	23.3	41.09	5.54	16.89
1.00	1.080	22.8	40.66	5.45	16.12
1.02	1.081	22.5	41.25	5.28	15.35
1.04	1.083	22.6	41.92	5.13	15.07
1.06	1.098	23.1	42.72	5.11	15.24
1.08	1.114	23.9	42.54	5.23	15.80
1.10	1.113	24.2	43.23	5.62	16.89
1.12	1.110	24.2	46.64	6.22	18.95
1.14	1.100	24.4	46.49	6.13	18.90
1.16	1.090	24.4	43.95	5.68	17.51
1.18	1.084	24.3	41.72	5.34	16.63
1.20	1.078	24.5	40.75	5.10	15.79
1.22	1.085	24.6	40.55	4.96	15.18
1.24	1.093	24.3	40.99	4.91	14.87
1.26	1.102	24.2	40.80	4.79	14.32
1.28	1.111	24.5	40.01	4.61	13.75
1.30	1.108	24.7	39.08	4.50	13.52
1.32	1.103	24.7	38.26	4.33	12.87
1.34	1.090	24.8	39.22	4.18	11.87
1.36	1.076	24.6	40.69	4.23	11.85
1.38	1.076	24.6	41.09	4.35	12.51
1.40	1.076	24.7	42.49	4.61	13.57
1.42	NA	24.6	43.25	4.67	13.63
1.44	NA	NA	43.53	4.63	13.41
1.46	NA	NA	NA	NA	NA
1.48	NA	NA	NA	NA	NA
1.50	NA	NA	NA	NA	NA
1.52	NA	NA	NA	NA	NA
1.54	NA	NA	NA	NA	NA
1.56	NA	24.6	45.38	3.74	10.06
1.58	1.084	24.9	44.69	4.07	11.15
1.60	1.090	25.0	42.98	4.27	11.80
1.62	1.096	24.7	42.03	4.18	11.74
1.64	1.084	24.1	42.63	4.08	11.99
1.66	1.072	23.5	42.86	4.12	12.88
1.68	1.077	23.1	42.51	4.05	12.89
1.70	1.084	23.0	41.72	3.47	10.54
1.72	1.091	22.7	43.83	3.59	10.21
1.74	1.099	22.3	48.06	4.33	11.93
1.76	1.106	22.0	46.69	4.24	11.80
1.78	1.114	22.1	42.41	3.90	11.60
1.80	1.119	22.6	39.69	3.52	11.28
1.82	1.123	23.4	38.56	3.44	11.37
1.84	1.117	24.0	38.38	3.35	11.19
1.86	1.110	24.4	38.10	3.25	10.64
1.88	1.107	24.5	38.24	3.24	10.22
1.90	1.104	24.4	38.57	3.27	10.27
1.92	1.105	24.3	38.68	3.21	9.90
1.94	1.106	24.5	37.67	2.99	8.88
1.96	1.098	24.9	37.77	3.24	9.82
1.98	1.088	25.0	37.43	3.45	10.52
2.00	1.072	25.1	37.10	3.53	11.04
2.02	1.058	25.3	38.04	3.67	11.91
2.04	1.081	25.3	39.62	3.75	12.46
2.06	1.106	25.5	42.03	3.98	13.38
2.08	1.110	26.0	40.21	3.77	12.03
2.10	1.112	26.4	38.06	3.31	10.17
2.12	1.110	26.4	38.62	3.14	9.59
2.14	1.107	26.1	38.37	2.97	8.78
2.16	1.098	25.9	38.20	2.92	8.54
2.18	1.090	25.6	39.06	3.03	8.87
2.20	1.106	25.1	40.39	2.88	8.43
2.22	1.122	24.5	42.48	2.85	8.69
2.24	1.110	24.2	42.43	2.94	9.10
2.26	1.096	23.6	41.69	3.25	9.61
2.28	1.079	22.5	42.45	3.82	11.12
2.30	1.064	21.9	44.77	4.05	12.77
2.32	1.072	21.6	48.17	4.36	14.88
2.34	1.080	21.4	50.23	4.87	16.82
2.36	1.068	21.1	48.51	4.69	16.08
2.38	1.055	21.1	47.60	4.37	15.58
2.40	1.060	21.0	49.88	4.84	17.41
2.42	1.065	20.5	52.21	5.35	18.91
2.44	1.058	20.4	53.46	5.54	19.37
2.46	1.050	20.6	56.04	6.09	20.78
2.48	1.050	21.0	57.12	6.37	21.52
2.50	1.051	21.1	54.00	5.90	20.12
2.52	1.072	20.9	50.23	5.25	18.40
2.54	1.093	21.0	54.55	5.80	20.37
2.56	1.076	21.4	58.10	6.28	21.93
2.58	1.057	21.7	57.76	6.18	21.35
2.60	1.052	22.1	56.16	5.89	20.29
2.62	1.049	22.2	54.74	5.88	20.10
2.64	1.066	22.4	51.88	5.77	19.68
2.66	1.083	22.5	48.46	5.16	18.42
2.68	1.081	22.4	48.63	4.63	17.36
2.70	1.077	22.2	48.85	4.21	15.83
2.72	1.078	22.3	47.93	4.14	15.33
2.74	1.080	22.1	47.84	3.93	14.09
2.76	1.086	22.1	48.16	3.60	12.97
2.78	1.091	22.4	47.66	3.42	12.63
2.80	1.076	22.5	48.22	3.54	13.56
2.82	1.060	22.4	48.25	3.78	14.66
2.84	1.052	22.3	48.12	3.79	14.45
2.86	1.044	22.5	47.01	3.19	12.27
2.88	NA	22.9	44.46	2.61	9.85
2.90	NA	NA	45.84	3.19	11.58
2.92	NA	NA	50.67	4.51	16.25
2.94	NA	NA	NA	NA	NA
2.96	NA	NA	NA	NA	NA
2.98	NA	NA	NA	NA	NA
3.00	NA	NA	NA	NA	NA
3.02	NA	NA	NA	NA	NA
3.04	NA	NA	NA	NA	NA
3.06	NA	26.4	37.17	2.16	5.79
3.08	1.102	27.2	37.39	2.29	6.38
3.10	1.100	28.1	36.44	2.52	7.13
3.12	1.098	28.7	35.59	2.67	7.34
3.14	1.113	29.0	35.81	2.59	6.93
3.16	1.128	28.7	36.54	2.57	6.99
3.18	1.126	28.0	37.24	2.79	7.96
3.20	1.122	27.2	38.41	2.88	8.37
3.22	1.120	26.6	40.46	3.06	9.16
3.24	1.117	25.6	43.43	3.57	11.09
3.26	1.095	24.7	47.87	4.58	14.68

Notes: GRA = gamma ray attenuation, MS = magnetic susceptibility, NA = not available. Only a portion of this table appears here. The complete table is available in **ASCII.**

Table T5. Depth mapping pairs from Site 1219 to 1218 (in rmcd).

Depth (rmcd)	
Site 1219	Site 1218
0.00	0.00
4.12	16.54
4.70	18.96
4.88	19.49
5.18	20.29
5.40	20.52
5.55	20.83
5.65	20.99
6.83	23.51
7.50	25.79
8.80	30.46
8.82	31.78
9.38	31.96
9.82	33.50
10.23	34.78
14.86	40.52
17.78	44.86
19.54	46.60
20.38	47.22
20.98	47.90
21.24	48.14
21.34	48.34
21.68	49.20
22.10	49.76
23.23	51.19
24.04	52.34
24.22	52.38
24.45	52.55
24.81	52.95
25.12	53.29
26.65	55.22
27.22	55.94
28.20	57.40
29.37	58.91
29.43	59.15
29.93	59.35
30.44	60.58
30.86	61.30
31.22	62.32
31.42	62.74
31.76	63.42
31.92	63.74
32.14	64.20
32.70	65.54
33.46	66.76
33.96	67.64
34.52	68.58
35.00	69.30
35.26	69.74
35.48	70.14
35.96	70.98
36.34	71.64
36.98	72.74
37.78	74.10
38.10	74.68
39.22	76.20
39.24	76.32
39.88	77.16
40.26	77.74
40.74	78.52
40.92	78.88
41.28	79.66
41.50	80.10
41.74	80.66
42.36	81.72
44.56	83.06
45.04	83.78
45.36	84.26
45.84	85.06
46.12	85.36
46.56	85.96
46.80	86.30
47.04	86.60
47.56	87.24
47.82	87.74
48.56	88.60
49.10	89.24
50.28	90.70
50.88	91.70
51.46	92.52
51.58	92.76
51.74	92.94
52.04	93.38
52.62	94.38
53.80	96.30
54.52	97.38
55.12	98.20
55.82	99.14
56.12	99.70
56.64	100.64
56.88	101.02
57.62	102.36
57.90	103.76
58.58	105.30
59.10	106.76
59.78	107.88
60.08	108.36
60.46	108.88
60.76	109.36
61.32	110.22
61.86	110.88
62.20	111.38
62.52	112.02
63.30	113.44
63.54	115.86
64.18	116.64
64.42	117.00
64.68	117.42
65.22	118.38
65.34	118.66
66.64	120.54
67.56	122.50
68.46	123.54
68.78	124.00
68.94	124.28
69.96	126.28
70.30	127.20
70.62	128.04
71.14	128.60
71.68	129.32
72.02	129.72
72.90	131.36
73.28	131.76
73.90	132.22
74.76	132.86
75.20	133.22
75.64	133.70
76.62	134.86
77.16	135.42
77.70	135.94
78.16	136.48
79.16	137.44
79.56	137.86
80.34	138.72
81.16	139.44
81.84	140.14
82.16	140.44
82.60	140.98
83.88	142.04
85.46	142.92
86.72	143.50
87.36	144.48
87.90	145.10
88.14	145.54
88.66	146.94
89.12	147.84
89.72	148.56
90.24	148.94
90.70	149.54
92.06	150.98
92.48	151.38
92.84	151.88
93.50	152.50
93.96	153.10
94.32	153.56
94.66	153.88
95.50	154.82
96.56	155.78
97.46	156.78
98.68	157.82
99.18	158.38
100.62	160.10
102.52	162.06
102.86	162.54
103.44	163.22
103.92	163.78
104.88	164.70
108.20	167.70
109.78	169.00
110.64	169.76
112.22	171.38
113.44	172.50
114.86	173.90
115.92	175.12
120.14	179.38
135.40	196.28
136.66	198.00
140.38	201.06
141.46	201.94
143.82	205.38
144.48	205.96
145.00	206.68
145.84	207.68
152.50	215.66
156.92	220.92
160.54	225.13
160.84	225.46
161.54	226.26
161.74	226.41
162.45	227.01
162.62	227.18
163.25	227.82
163.50	228.00
164.30	228.75
164.65	229.02
164.95	229.26
165.11	229.38
165.77	229.95
165.92	230.10
166.28	230.37
166.68	230.69
166.98	231.00
167.04	231.06
167.20	231.18
167.70	231.82
168.16	232.27
168.53	232.54
168.79	232.84
169.08	233.17
170.14	234.22
170.43	234.67
171.14	236.95
171.90	237.82
172.06	238.12
172.17	238.36
172.50	238.69
172.81	239.11
173.08	239.65
173.30	240.07
173.40	240.44
174.40	240.94
174.86	241.50
177.66	244.52
180.18	247.22
187.30	252.92
189.04	254.84
193.06	257.42
193.40	257.68
194.32	258.90
196.78	260.84
199.00	262.70
200.06	263.90
203.42	267.24
203.78	267.48
207.86	270.64
208.96	271.56
212.04	274.34
213.42	276.18
214.04	276.76
214.40	277.12
216.06	278.92
218.74	281.20
219.58	282.40
219.96	283.12
220.50	283.80
221.32	284.90
221.84	285.62
222.42	286.34
223.84	290.12
224.04	290.68
224.40	291.12
224.58	291.34
225.38	292.52
226.32	293.74
227.72	296.24
228.40	296.74
229.98	298.12

Note: This table is also available in **ASCII.**

Table T6. Magnetochrons for Site 1218 and 1219, on rmcd depth scale. (**See table notes.** Continued on next two pages.)

Top, Bottom	Chron	Site 1219 mid (rmcd)	Site 1219 mid 1218 equivalent (rmcd)	Site 1218 mid (rmcd)	Site 1219 top (rmcd)	Site 1219 base (rmcd)	Site 1218 top (rmcd)	Site 1218 base (rmcd)
T	C1n							
B	C1n	*1.00*	*4.01*	*5.44*	*0.90*	*1.10*		
T	C1r.1n	*1.18*	*4.72*	*7.79*	*1.15*	*1.20*		
B	C1r.1n	*1.33*	*5.32*	*8.31*	*1.25*	*1.40*		
T	C1r.2n							
B	C1r.2n							
T	C2n	*2.10*	*8.43*	*10.02*	*2.00*	*2.20*		
B	C2n	*2.33*	*9.33*	*11.73*	*2.20*	*2.45*		
T	C2An.1n	*2.98*	*11.94*	*13.78*	*2.85*	*3.10*		
B	C2An.1n							
T	C2An.2n							
B	C2An.2n							
T	C2An.3n			*16.28*				
B	C2An.3n	*3.85*	*15.46*	*17.98*	*3.80*	*3.90*		
T	C3n.1n	*4.70*	*18.95*	*18.96*	*4.60*	*4.80*	*18.81*	*19.10*
B	C3n.1n	*4.88*	*19.49*	*19.49*	*4.80*	*4.95*	*19.43*	*19.54*
T	C3n.2n	*5.18*	*20.28*	*20.29*	*5.10*	*5.25*	*20.24*	*20.33*
B	C3n.2n	*5.40*	*20.52*	*20.52*	*5.30*	*5.50*	*20.48*	*20.56*
T	C3n.3n	*5.55*	*20.83*	*20.83*	*5.50*	*5.60*	*20.77*	*20.88*
B	C3n.3n	*5.65*	*20.99*	*20.99*	*5.60*	*5.70*	*20.94*	*21.03*
T	C3n.4n			*21.28*			*21.23*	*21.32*
B	C3n.4n			*21.68*			*21.58*	*21.78*
T	C3An.1n	*6.83*	*23.51*	*23.51*	*6.75*	*6.90*	*23.40*	*23.62*
B	C3An.1n			*24.24*			*24.18*	*24.29*
T	C3An.2n			*24.76*			*24.66*	*24.85*
B	C3An.2n	*7.50*	*25.78*	*25.79*	*7.45*	*7.55*	*25.65*	*25.92*
T	C3Bn			*27.03*			*28.45*	*28.63*
B	C3Bn			*27.27*			*29.72*	*29.89*
T	C3Br.1n			*27.31*				
B	C3Br.1n			*27.44*				
T	C3Br.2n							
B	C3Br.2n							
T	C4n.1n	*8.80*	*30.45*	*30.46*	*8.65*	*8.95*	*30.37*	*30.54*
B	C4n.1n			*30.61*			*30.59*	*30.63*
T	C4n.2n			*30.87*			*30.76*	*30.98*
B	C4n.2n	*9.38*	*31.96*	*31.96*	*9.25*	*9.50*	*31.72*	*32.20*
T	C4r.1n							
B	C4r.1n							
T	C4An							
B	C4An							
T	C4Ar.1n			*33.11*			*32.98*	*33.23*
B	C4Ar.1n			*33.52*			*33.43*	*33.60*
T	C4Ar.2n			*33.96*			*33.85*	*34.06*
B	C4Ar.2n			*34.49*			*34.43*	*34.55*
T	C5n.1n			*34.78*			*34.68*	*34.88*
B	C5n.1n	*12.15*	*37.16*		*11.80*	*12.50*		
T	C5n.2n							
B	C5n.2n							
T	C5r.1n			*36.19*			*36.17*	*36.21*
B	C5r.1n			*36.52*			*36.46*	*36.58*
T	C5r.2n			*37.82*			*37.58*	*37.86*
B	C5r.2n			*38.07*			*38.03*	*38.20*
T	C5An.1n			*38.97*			*38.86*	*38.94*
B	C5An.1n			*39.33*			*39.35*	*39.44*
T	C5An.2n			*39.64*			*39.64*	*39.73*
B	C5An.2n			*40.18*			*40.51*	*40.64*
T	C5Ar.1n			*41.22*			*41.18*	*41.26*
B	C5Ar.1n			*41.38*			*41.30*	*41.46*
T	C5Ar.2n			*41.66*			*41.55*	*41.67*
B	C5Ar.2n			*41.85*			*41.80*	*41.92*
T	C5AAn			*42.30*			*42.21*	*42.38*
B	C5AAn			*42.77*			*42.71*	*42.96*
T	C5ABn			*43.23*			*43.08*	*43.29*
B	C5ABn			*43.95*			*43.78*	*43.95*
T	C5ACn			*44.29*			*44.12*	*44.40*
B	C5ACn			*44.99*			*44.86*	*44.02*

Table T6 (continued).

Top, Bottom	Chron	Site 1219 mid (rmcd)	Site 1219 mid 1218 equivalent (rmcd)	Site 1218 mid (rmcd)	Site 1219 top (rmcd)	Site 1219 base (rmcd)	Site 1218 top (rmcd)	Site 1218 base (rmcd)
T	C5ADn			*45.11*			*45.07*	*45.15*
B	C5ADn			*46.16*			*46.02*	*46.23*
T	C5Bn.1n			46.64			46.47	46.64
B	C5Bn.1n			46.85			46.76	46.97
T	C5Bn.2n	20.38	47.22	47.20	20.30	20.45	47.10	47.34
B	C5Bn.2n	20.83	47.73	47.62	20.70	20.95	47.55	47.72
T	C5Cn.1n	23.23	51.19	51.19	23.16	23.30	51.13	51.26
B	C5Cn.1n	24.04	52.34	52.34	23.91	24.17	52.00	52.05
T	C5Cn.2n	24.22	52.38	52.38	24.17	24.27	52.14	52.39
B	C5Cn.2n	24.45	52.55	52.55	24.32	24.57	52.53	52.61
T	C5Cn.3n	24.81	52.95	52.95	24.69	24.92	52.88	52.96
B	C5Cn.3n	25.12	53.29	53.29	25.02	25.22	53.27	53.40
T	C5Dn	26.65	55.21	55.22			55.14	55.36
B	C5Dn	27.22	55.94	55.94			55.93	56.14
T	C5Dr.1n	27.43	56.25					
B	C5Dr.1n	27.53	56.40					
T	C5En	28.20	57.39	57.40			57.28	57.58
B	C5En	29.37	58.91	58.91			59.06	59.24
T	C6n	29.93	59.35	59.35			59.76	59.85
B	C6n	33.46	66.75	66.76			66.64	67.01
T	C6An.1n	35.06	69.39	69.30			69.26	69.38
B	C6An.1n	35.63	70.39	70.25			70.21	70.46
T	C6An.2n	36.28	71.53	71.43			71.16	71.49
B	C6An.2n	37.28	73.24	73.16			73.15	73.69
T	C6AAn	39.94	77.25	76.71			76.01	76.62
B	C6AAn	40.27	77.75	77.68			77.63	77.80
T	C6AAr.1n	42.39	81.74	81.20				
B	C6AAr.1n	43.14	82.20	82.57				
T	C6AAr.2n	45.09	83.86	83.89			83.81	83.94
B	C6AAr.2n	45.49	84.48	84.31			84.25	84.38
T	C6Bn.1n	45.99	85.22	85.05			84.99	85.08
B	C6Bn.1n	46.89	86.41	86.34			86.30	86.43
T	C6Bn.2n	47.16	86.75	86.74			86.73	86.82
B	C6Bn.2n	49.16	89.31	89.48			89.45	89.87
T	C6Cn.1n	51.46	92.51	92.48			92.27	92.59
B	C6Cn.1n	52.12	93.52	93.37			93.32	93.58
T	C6Cn.2n	53.04	95.06	94.91			94.42	95.15
B	C6Cn.2n	53.80	96.29	96.20			96.04	96.41
T	C6Cn.3n	55.58	98.81	98.80			98.65	98.86
B	C6Cn.3n	56.09	99.63	99.62			99.59	100.85
T	C7n.1n	59.18	106.88	106.87			106.81	106.92
B	C7n.1n	59.40	107.25	107.18			107.12	107.23
T	C7n.2n	60.05	108.31	108.02			107.72	108.32
B	C7n.2n	62.39	111.75	111.59			111.37	111.81
T	C7An	63.73	116.09	115.49	63.16	64.29	115.37	115.60
B	C7An	64.63	117.33	117.88	64.54	64.71	117.73	118.03
T	C8n.1n	65.92	119.49	119.49	65.74	66.09	119.41	119.56
B	C8n.1n	67.32	121.98	121.59	67.24	67.39	121.47	121.70
T	C8n.2n	67.62	122.56	122.12	67.44	67.79	122.00	122.23
B	C8n.2n	72.55	130.70	131.27	72.09	73.00	131.00	131.53
T	C9n	79.41	137.70	137.33	79.18	79.63	136.60	138.05
B	C9n	92.87	151.91	151.63	92.67	93.07	151.47	151.78
T	C10n.1n	98.80	157.95	157.84	98.47	99.12	157.72	157.95
B	C10n.1n	101.87	161.39	161.20	101.57	102.17	160.93	161.46
T	C10n.2n	102.60	162.17	162.18	102.37	102.82	161.99	162.37
B	C10n.2n	104.30	164.14	164.02	104.02	104.57	163.90	164.13
T	C11n.1n			178.45			178.36	178.53
B	C11n.1n			184.41			184.28	184.54
T	C11n.2n			185.11			184.93	185.28
B	C11n.2n			191.43			189.73	193.12
T	C12n	138.45	199.47	200.40	137.85	139.05	199.05	201.75
B	C12n	143.03	204.22	204.67	142.80	143.25	204.54	204.80
T	C13n	169.80	233.88					
B	C13n	173.36	240.29					
T	C15n	179.96	246.98					
B	C15n	180.56	247.52					
T	C16n.1n	181.08	247.94					

Table T6 (continued).

Top, Bottom	Chron	Site 1219 mid (rmcd)	Site 1219 mid 1218 equivalent (rmcd)	Site 1218 mid (rmcd)	Site 1219 top (rmcd)	Site 1219 base (rmcd)	Site 1218 top (rmcd)	Site 1218 base (rmcd)
B	C16n.1n	182.56	249.13					
T	C16n.2n	182.96	249.45					
B	C16n.2n	187.36	252.99					
T	C17n.1n	188.86	254.64					
B	C17n.1n	193.94	258.40		193.89	193.99		
T	C17n.2n	194.89	259.35		194.69	195.09		
B	C17n.2n	196.09	260.30		195.84	196.34		
T	C17n.3n	196.44	260.57		196.29	196.59		
B	C17n.3n	197.49	261.43		197.29	197.69		
T	C18n.1n	198.97	262.67		198.69	199.24		
B	C18n.1n	207.00	269.97		206.87	207.12		
T	C18n.2n	207.47	270.34		207.37	207.57		
B	C18n.2n	211.50	273.85		211.27	211.72		
T	C19n	224.37	291.08		224.09	224.64		
B	C19n	226.04	293.38		225.89	226.19		
T	C20n	232.29			232.19	232.39		
B	C20n	244.12			243.64	244.59		

Notes: Italics indicate less certain correlations. This table is also available in **ASCII.**

Table T7. Site 1218 calcareous nannofossils on rmcd depth scale.

Event	Mid-depth (rmcd)	Error (rmcd)	Hole	Core, section, interval (cm)		Depth			
				Top	Base	Top (mbsf)	Base (mbsf)	Top (rmcd)	Base (rmcd)
			199-						
B *Discoaster kugleri*	40.28	0.16	1218B	5H-2, 56	5H-2, 88	34.46	34.78	40.12	40.44
B *Catinaster coalitus*	41.33	0.43	1218A	4H-7, 50	4H-CC	36.70	37.08	40.90	41.75
T *Cyclicargolithus floridanus*	48.07	0.32	1218B	5H-7, 45	5H-CC	41.85	42.42	47.75	48.38
T *Sphenolithus heteromorphus*	50.93	0.28	1218A	5H-7, 15	5H-CC	45.85	46.40	50.65	51.20
T *Discoaster deflandrei* acme	50.93	0.28	1218A	5H-7, 15	5H-CC	45.85	46.40	50.65	51.20
T *Triquetrorhabdulus carinatus*	63.63	1.28	1218A	6H-CC	7H-1, 120	55.32	56.90	62.35	64.91
T *Triquetrorhabdulus carinatus* acme	87.51	0.25	1218A	9H-2, 80	9H-2, 130	77.00	77.50	87.26	87.76
B *Sphenolithus disbelemnos*	90.51	0.25	1218A	9H-4, 80	9H-4, 130	80.00	80.50	90.26	90.76
B *Discoaster druggii*	92.46	0.20	1218A	9H-5, 130	9H-6, 20	82.00	82.40	92.26	92.66
T *Sphenolithus delphix*	97.00	0.40	1218B	10H-4, 140	10H-5, 70	85.80	86.60	96.60	97.40
T *Sphenolithus delphix*	97.55	0.11	1218A	10H-1, 140	10H-2, 10	85.60	85.80	97.44	97.65
B *Sphenolithus delphix*	99.25	0.35	1218B	10H-6, 70	10H6, 140	88.10	88.80	98.90	99.60
B *Sphenolithus delphix*	100.40	0.10	1218A	10H-3, 120	10H-3, 140	88.40	88.60	100.30	100.50
T *Sphenolithus ciperoensis*	110.33	0.75	1218B	11H-5, 80	11H-6, 80	96.20	97.70	109.58	111.08
T *Sphenolithus ciperoensis*	110.56	0.71	1218A	11H-2, 130	11H-3, 130	96.50	98.00	109.85	111.27
T *Cyclicargolithus abisectus* acme	113.19	0.29	1218A	11H-4, 130	11H-5, 38	99.50	100.08	112.90	113.48
T *Sphenolithus distentus*	131.99	0.57	1218A	13H-3, 75	13H-4, 45	116.45	117.65	131.42	132.56
T *Dictyococcites bisectus*	132.53	0.34	1218B	13H-6, 80	13H-6, 148	116.70	117.38	132.19	132.87
T *Sphenolithus distentus*	132.54	0.15	1218B	13H-6, 100	13H-6, 130	116.90	117.20	132.39	132.69
B *Sphenolithus ciperoensis*	145.17	0.75	1218A	14H-5, 80	14H-6, 80	129.00	130.50	144.42	145.92
B *Sphenolithus ciperoensis*	146.32	0.10	1218B	15H-1, 100	15H-1, 120	128.40	128.60	146.22	146.42
B *Sphenolithus distentus*	190.58	0.70	1218A	18H-CC	19H-1, 120	169.54	170.90	189.87	191.28
T *Reticulofenestra umbilicus* ≥14 µm	220.85	0.38	1218A	22X-2, 70	22X-2, 147	198.10	198.87	220.47	221.23
T *Ericsonia formosa*	231.91	0.19	1218A	23X-2, 148	23X-3, 35	208.48	208.85	231.72	232.09
T *Discoaster saipanensis*	244.57	0.06	1218A	24X-4, 78	24X-4, 90	219.98	220.10	244.51	244.62
T *Discoaster barbadiensis*	245.79	0.13	1218A	24X-5, 56	24X-5, 85	221.26	221.55	245.66	245.91
T *Chiasmolithus grandis*	260.27	0.21	1218A	25X-7, 70	25X-CC	233.90	234.31	260.06	260.48
B *Dictyococcites bisectus*	268.01	1.04	1218A	26X-5, 60	26X-6, 125	240.90	243.05	266.97	269.05
T *Chiasmolithus solitus*	277.82	1.58	1218A	27X-CC	28X-1, 50	250.11	254.00	276.24	279.40
T *Nannotetrina* spp.	298.78	0.31	1218A	30X-2, 90	30X-3, 2	273.10	273.72	298.47	299.09

Notes: T = top, B = bottom. This table is also available in **ASCII.**

Table T8. Site 1219 calcareous nannofossils on (rmcd) depth scale.

Event	Depth (mid) (rmcd)	±	Site/Hole	Core, section, interval (cm) Top	Core, section, interval (cm) Base	Depth Top (mbsf)	Depth Base (mbsf)	Depth Top (rmcd)	Depth Base (rmcd)	Depth (mid) 1218 (rmcd)	±
			199-1219-								
T *Cyclicargolithus floridanus*	19.71	0.23	A	3H-3, 92	3H-3, 138	19.42	19.88	19.48	19.93	46.72	0.17
T *Sphenolithus heteromorphus*	20.71	0.78	A	3H-3, 138	3H-4, 145	19.88	21.45	19.93	21.48	47.59	0.90
T *Discoaster deflandrei* acme	22.71	0.94	A	3H-5, 25	3H-6, 26	21.75	23.62	21.77	23.64	50.53	1.23
T *Triquetrorhabdulus carinatus*	31.54	0.24	A	4H-4, 92	4H-4, 140	30.42	30.90	31.30	31.78	62.98	0.49
T *Triquetrorhabdulus carinatus* acme	47.84	1.08	A	5H-CC	6H-1, 90	44.47	44.90	46.76	48.91	87.76	1.39
B *Sphenolithus disbelemnos*	50.40	0.32	A	6H-2, 40	6H-2, 105	45.90	46.55	50.08	50.71	90.89	0.48
T *Sphenolithus delphix*	53.78	0.92	B	4H-CC	5H-1, 30	48.75	49.80	52.86	54.70	96.27	1.43
T *Sphenolithus delphix*	54.64	0.29	A	6H-5, 30	6H-5, 90	50.30	50.90	54.35	54.93	97.54	0.41
B *Sphenolithus delphix*	56.75	0.05	B	5H-2, 80	5H-2, 90	51.80	51.90	56.70	56.80	100.81	0.08
B *Sphenolithus delphix*	56.80	0.20	A	6H-6, 120	6H-7, 20	52.70	53.20	56.60	56.99	100.89	0.33
T *Sphenolithus ciperoensis*	61.83	0.38	A	7H-5, 10	7H-5, 80	59.44	60.14	61.45	62.20	110.84	0.50
T *Cyclicargolithus abisectus* acme	63.10	0.90	A	7H-5, 80	7H-6, 90	60.14	61.74	62.20	64.00	113.08	2.52
T *Sphenolithus ciperoensis*	63.98	0.16	B	5H-CC	6H-1, 60	58.79	59.60	63.81	64.14	116.39	0.20
T *Sphenolithus distentus*	70.80	0.75	A	8H-3, 100	8H-4, 100	67.00	68.50	70.05	71.55	128.23	1.31
B *Sphenolithus ciperoensis*	83.52	0.75	A	9H-2, 140	9H-3, 140	75.40	76.90	82.77	84.27	141.74	0.57
T *Sphenolithus pseudoradians*	121.04	0.73	A	12H-5, 80	12H-6, 80	107.80	109.30	120.31	121.77	180.38	0.81
T *Sphenolithus pseudoradians*	121.95	0.16	B	11H-3, 85	11H-3, 120	110.35	110.70	121.78	122.11	181.38	0.18
B *Sphenolithus distentus*	131.27	0.77	A	13H-3, 80	13H-4, 80	113.86	115.36	130.49	132.04	191.70	0.86
T *Reticulofenestra umbilicus* ≥14 µm	156.98	0.10	A	15H-5, 140	15H-6, 10	136.90	137.10	156.88	157.08	220.99	0.12
T *Reticulofenestra umbilicus* ≥14 µm	159.00	0.15	B	14H-7, 40	14H-7, 70	144.40	144.70	158.85	159.15	223.34	0.17
T *Ericsonia formosa*	167.23	0.78	A	16H-4, 140	16H-5, 140	144.96	146.51	166.45	168.00	231.21	0.80
T *Ericsonia formosa*	167.56	0.15	B	15H-5, 76	15H-5, 104	150.82	151.10	167.41	167.71	231.64	0.19
T *Discoaster saipanensis*	187.22	13.83	A	17H-2, 90	19H-7, 5	150.90	176.55	173.39	201.04	252.85	12.24
T *Discoaster barbadiensis*	187.22	13.83	A	17H-2, 90	19H-7, 5	150.90	176.55	173.39	201.04	252.85	12.24
T *Chiasmolithus grandis*	188.51	15.12	A	17H-2, 90	20H-1, 114	150.90	178.14	173.39	203.63	254.26	13.49
B *Dictyococcites bisectus*	210.69	6.18	A	20H-2, 52	21H-3, 80	179.02	190.30	204.51	216.86	273.12	5.78
T *Dictyococcites hesslandii*	210.69	6.18	A	20H-2, 52	21H-3, 80	179.02	190.30	204.51	216.86	273.12	5.78
B *Reticulofenestra umbilicus* ≥14 µm	227.36	0.38	A	22H-3, 49	22H-3, 125	199.49	200.25	226.98	227.74	295.60	0.67
P *Nannotetrina* spp.	239.09	5.76	A	22H-CC	24H-1, 36	205.84	215.36	233.33	244.85		
P *Nannotetrina alata*	244.09	0.47	A	23H-7, 63	24H-1, 6	215.13	215.06	243.62	244.55		
X *T. contortus/T. orthostylus*	266.43	0.24	A	26X-1, 60	26X-1, 107	234.70	235.17	266.19	266.66		
T-T *T. contortus/F. tympaniformis*	273.26	4.15	A	26X-3, 52	27X-CC	237.62	244.92	269.11	277.41		

Notes: T = top, B = bottom. This table is also available in **ASCII.**

Table T9. Depth re-mapping pairs from Site 1218 core (rmcd) to 1218 logging (mbsf).

Depth	
(rmcd)	(lmbsf)
199-1218-	
0.00	0.00
87.22	78.84
91.96	82.73
103.42	89.89
113.26	98.12
127.78	112.47
132.04	116.31
137.14	120.95
138.70	122.20
140.48	123.70
142.54	125.73
151.04	131.27
152.26	132.41
153.76	133.73
155.28	135.94
156.80	137.46
157.78	138.61
158.80	139.57
161.12	142.04
163.12	143.56
164.88	145.79
167.32	148.41
169.02	149.88
172.36	151.74
172.96	152.40
174.60	153.97
177.88	157.73
179.40	158.95
181.64	160.09
184.14	161.21
186.26	164.29
187.60	166.11
189.96	168.15
192.52	169.82
197.36	173.51
200.96	178.15
203.26	180.41
205.50	182.80
209.02	186.21
211.40	187.65
213.28	189.38
215.70	191.74
216.02	192.35
217.36	193.09
220.42	196.65
221.30	197.48
222.14	198.12
223.48	198.93
226.76	200.84
227.42	201.57
230.52	205.03
231.80	206.35
234.54	208.23
235.32	209.37
239.58	212.39
241.38	214.09
242.14	214.53
243.82	216.08
244.74	216.79
246.38	218.24
248.08	219.99
252.20	223.85
264.76	237.18
277.70	251.66
281.48	254.89
286.92	259.76
302.17	281.20

Note: This table is also available in **ASCII.**

CHAPTER NOTES*

N1. After final pages had been printed for Vol. 199 of the *Scientific Results of the ODP Proceedings,* an error was found in Table T2. The values in the "mcd" and "rmcd" columns were reversed. The error is corrected in this electronic volume.

*Dates reflect file corrections or revisions.